Temperature dependences for air-broadened Lorentz half width and pressure-shift coefficients in the 30013←00001 and 30012←00001 bands of CO_2 near 1600 nm

*A. Predoi-Cross[1] *, A.R.W. McKellar[2], D. Chris Benner[3], V. Malathy Devi[3]*

R. R. Gamache[4], C. E. Miller[5], R. A. Toth[5] and L. R. Brown[5]

[1]Department of Physics and Astronomy, University of Lethbridge, Lethbridge, AB, Canada; [2]Steacie Institute for Molecular Sciences, National Research Council of Canada, Ottawa, ON, Canada; [3]The College of William and Mary, Williamsburg, VA, USA; [4]Department of Environmental, Earth, and Atmospheric Sciences, University of Massachusetts Lowell; [5]Jet Propulsion Laboratory, Pasadena, California Institute of Technology CA, USA

*** Corresponding author:**

Dr. Adriana Predoi-Cross

Department of Physics and Astronomy, University of Lethbridge

4401 University Drive, Lethbridge, AB, T1K 3M4 Canada

E-mail address: adriana.predoicross@uleth.ca

PACS classification: 32.70.Jz, 33.70.Jg, 33.20.Ea

ABSTRACT

In this study 39 high resolution spectra of air-broadened CO_2 recorded at temperatures between 215 and 294 K were analyzed using a multispectrum nonlinear least squares technique to determine temperature dependences of air-broadened Lorentz half width and air-induced pressure shift coefficients for over 100 individual $^{12}C^{16}O_2$ transitions in the 30012←00001 (at 6348 cm^{-1}) and 30013←00001 (at 6228 cm^{-1}) bands. Data were recorded with two different Fourier transform spectrometers (Kitt Peak FTS at the National Solar Observatory in Arizona and the Bomem FTS at NRC, Ottawa) with absorption path lengths ranging between 25 m and 121 m. The sample pressures varied between 11 torr (pure CO_2) and 924 torr (CO_2-air) with volume mixing ratios of CO_2 in air between ~ 1.5 % and 11 %. To minimize systematic errors and increase the accuracy of the retrieved parameters, a constrained multispectrum nonlinear least squares fitting technique was used to include theoretical quantum mechanical expressions for the rovibrational energies and intensity parameters rather than retrieving the individual positions and intensities line-by-line. The results suggest no detectable vibrational dependence for the temperature dependences for the air-broadened Lorentz half width coefficients and the air-induced pressure shift coefficients. The half width coefficients and temperature dependence exponents were modeled using semiclassical calculations based upon the Robert-Bonamy formalism. A good agreement is seen between the measurements and theoretical calculations. Beyond $|m|$ = 26, a simple scaling factor (0.96) has been applied to the calculated half width coefficients to match the experimental measurements.

.

Key Words: carbon dioxide, air-broadening, temperature dependence, near infrared, multispectrum fitting, pressure shifts, theoretical calculations

1. Introduction

The Earth's atmosphere bears the fingerprint of human influences. Our knowledge and understanding of spatial and temporal patterns in the Earth's carbon cycle, and ultimately of global warming and climate change, are directly linked to our ability to monitor the atmospheric CO_2, a well mixed greenhouse gas with a very long lifetime. A crucial objective in monitoring a greenhouse gas is to understand the spatial and temporal fluctuations in surface fluxes.

Satellite-based remote sensing of CO_2 can provide a global distribution of its concentrations with a precision better than 1%. Such a precision is difficult to achieve due to the fact that the changes in the surface pressure can affect the retrievals of column concentrations of CO_2 more than the natural variations due to its sources and sinks. Currently there are several satellite remote sounding instruments designed to measure column concentrations of CO_2 (e. g. the Atmospheric Infrared Sounder (AIRS) [1] and the Infrared Atmospheric Sounder Interferometer (IASI) [2]) using mid-infrared wavelengths; next year two more (the Orbiting Carbon Observatory (OCO) [3] and the Greenhouse Gases Observing Satellite (GOSAT) [4]) are scheduled for launch which will target near-IR transitions of CO_2, particularly those near 1.6 μm. For tropospheric remote sensing, reliable pressure broadening spectroscopy is essential. For the new missions like OCO and GOSAT, accuracies better than 1% are needed for the CO_2 air-broadening coefficients. Unfortunately, the temperature dependence coefficients for air broadening of all CO_2 bands used by the atmospheric community come from unpublished and unconfirmed predictions made 18 years ago [5].

To satisfy the new requirements, studies were undertaken to obtain air-broadened Lorentz widths of CO_2 at room temperature. The most extensive study was that by Toth et al. [6] who reported air-broadened half width and air-induced pressure shift coefficients for over 400 transitions belonging to 11 $^{12}CO_2$ bands between 4750 and 7000 cm^{-1}. In contrast, no past infrared measurements were available for the temperature dependence of air-broadened CO_2 widths, as seen in Table 1. Instead, the older studies obtained self-, N_2-, O_2- and Ar-broadening at different temperatures, and most reported values for relatively few transitions. Many of these [6-18] involved mid-infrared bands; only two studies [19, 20] considered temperature dependence in $30012 \leftarrow 00001$ at 6348 cm^{-1} and $30013 \leftarrow 00001$ at 6228 cm^{-1}. Significantly, most of the temperature dependence analyses assumed Voigt line shapes.

Subsequently, independent studies at room temperature [21-24] found that Voigt profiles were insufficient to reproduce observed line shapes in high quality laboratory spectra. Devi et al. [21, 22] measured the 30012 ← 00001 and 30013 ← 00001 bands using comprehensive multispectrum nonlinear least squares and concluded that the best results were obtained using a Speed Dependent Voigt (SDV) profile with line mixing effects determined via the relaxation matrix formalism [25]. Following this, Predoi-Cross et al. [23, 24] published an independent room-temperature study of air- and self- broadening, shifts, and weak (Rosenkranz) line mixing coefficients for transitions of the same two bands, using spectra from a different spectrometer and a different multispectrum retrieval software. The absorption profiles were analyzed using both Voigt and speed-dependent Voigt profiles with an associated asymmetric component due to line mixing. The air-broadened half width and line mixing coefficients were then modeled using the Energy Power Gap (EPG) and Energy Corrected Sudden (ECS) scaling laws. One difference in the two sets of studies was that in Devi et al. [21, 22] the retrieval technique was modified to adjust the rovibrational constants and intensity parameters (including Herman–Wallis terms) of the entire band(s) in the fitted interval rather than to retrieve individual positions and intensities of the transitions, as was done by Predoi-Cross et al. [23, 24].

In one sense, the present study extends these multispectrum analyses to obtain the temperature dependence of air broadening coefficients (half widths and pressure shifts) for 30012 ← 00001 and 30013 ← 00001 bands of carbon dioxide. The broadening coefficients (widths, shifts and temperature dependences) were retrieved simultaneously using 39 spectra obtained with two different spectrometers. The positions, intensities, line mixing and speed-dependent Voigt coefficients were constrained to the values obtained by Devi et al. [21, 22]. The temperature dependence coefficients of the air-induced pressure shifts were obtained for the first time. The measured air-broadened half width coefficients and their temperature dependence exponents were found to be in satisfactory agreement with theoretical values.

2. Experimental Details

The experiments described in this work were carried out using two different Fourier Transform Spectrometers (FTS). The spectra with path lengths of 24.94, 49 and 121.2 m were recorded at ~0.011 cm^{-1} resolution with the Kitt Peak FTS and are part of the data set used in Refs. [21, 22]. The long absorption paths were achieved using a 6-m base path White cell. The atmospheric path between the White cell and the entrance aperture of the FTS was purged with liquid nitrogen vapors through appropriate plexiglass tubings to minimize strong absorption features arising from CO_2 and H_2O. Other experimental details are given in Toth et al. [6, 26].

All other spectra were recorded at the Steacie Institute for Molecular Sciences at the National Research Council in Ottawa using a Bomem DA3.002 Fourier Transform Spectrometer. The experimental details are very similar to those of the room temperature study in Refs. [23, 24]. The spectra were recorded at nominal spectral resolutions of 0.008 and 0.009 cm^{-1}. A large multiple-traversal gas cell as described in Refs. [34, 35] and listed in [23] with a base length of 5 m gave absorption paths of 40.15 to 80.15 m. A total of 26 spectra recorded between 215.3 and 296.0 K with sample pressures varying from 59.8 to 798.0 torr, as summarized in Table 2, were combined with the 13 Kitt Peak spectra. Each spectrum represented the average of 24 to 32 interferograms, with a total data acquisition time of approximately 2 hours.

The cell, which sits entirely inside a vacuum jacket, was cooled by means of methanol from a refrigerated cooling bath (Neslab Model ULT-80DD) which circulated through copper coils soldered to the outside of the cell. The gas temperature was monitored with readings from platinum resistance thermometers mounted on the cooling lines and inside the cell, as well as from the temperature of the cooling bath itself. We estimated the accuracy of the temperature determination to be ± 0.5 K, with a further uncertainty of ± 0.5 K due to possible variations along the 5 m length of the cell. The uncertainties and possible inhomogeneties were greatest at the lowest temperature of 215 K. The temperatures were checked spectroscopically using several line intensities retrieved in Ref. 23, with an estimated accuracy of ± 0.2 K. The readings of the temperature monitor were corrected accordingly. As expected, the largest offset between the average temperature determined in this manner and that given by the temperature monitor was obtained at the lowest temperature.

The air and CO_2 gas mixture was taken from a pre-mixed commercial cylinder (BOC Gases Canada) and had a quoted volume mixing ratio of 0.096 CO_2 with an uncertainty of 2 %. The volume mixing ratio in each of the 26 spectra was determined by fitting these spectra first individually and finally simultaneously with the 13 Kitt Peak spectra such that the intensities of all transitions were identical to those reported in Refs. [21, 22] by constraining the rovibrational and intensity parameters for all bands appearing in each fitted interval. The revised values of the volume mixing ratios are reported in the table of experimental details (Table 2).

3. Spectroscopic Analysis

In each fitted interval (6120 – 6280 cm^{-1} for 30013 ← 00001 and 6280 – 6395 cm^{-1} for 30012 ← 00001), the line parameters were retrieved using nonlinear multispectrum curve fitting technique [27] modified with constraints on positions and on intensities, as was done in Refs. [21, 22]. Briefly, the software adjusted the constants in (1) for positions:

$$\begin{aligned} \nu_i &= G' - G'' + (B'J'[J'+1] - D'\{J'[J'+1]\}^2 + H'\{J'[J'+1]\}^3) \\ &\quad - (B''J''[J''+1] - D''\{J''[J''+1]\}^2 + H''\{J''[J''+1]\}^3) \end{aligned} \tag{1}$$

and in (2) and (3) for intensities

$$S_i = \frac{S_v \nu_i L_i F}{Q_r \nu_0} \exp\left(\frac{-C_2 E''}{T_0}\right)\left[1 - \exp\left(\frac{-C_2 \nu_i}{T_0}\right)\right] \tag{2}$$

where,

$$F = (1 + a_1 m + a_2 m^2 + a_3 m^3 + a_4 J'(J'+1))^2 \tag{3}$$

In (1) to (3), ν_i denotes the wavenumber (cm^{-1}) of the i^{th} transition, and prime and double prime denote the upper and lower vibrational levels, respectively. In (2), L_i are the Hönl-London factors and C_2 represents the second radiation constant; m is defined as $-J''$ in the P branch, $J''+1$ in the R branch and zero in the Q branch. Other terms have their usual meanings. The terms a_1 and a_2 in (3) were sufficient to describe the bands to the noise level of the spectra once the speed dependence and line mixing were utilized. The temperature dependences of pressure-broadened half width and shift coefficients were determined using the expressions given below:

$$b_L(p,T) = p\left[b_L^0(air)(p_0,T_0)(1-\chi)\left[\frac{T_0}{T}\right]^{n_a} + b_L^0(self)(p_0,T_0)\chi\left[\frac{T_0}{T}\right]^{n_s} \right] \tag{4}$$

$$\nu = \nu_0 + p\left[\delta^0(air)(1-\chi) + \delta^0(self)\chi\right] \tag{5}$$

$$\delta(T) = \delta^0(T_0) + \delta'(T - T_0) \tag{6}$$

In (4) to (6), b_L^0 and δ^0 represent pressure broadening and pressure shift coefficients (in $cm^{-1}atm^{-1}$ at 296 K), respectively. b_L (p, T) is the Lorentz half width (in cm^{-1}) of the spectral line at pressure p and temperature T, and $b_L^0(Gas)(p_0, T_0)$ is the Lorentz half width coefficient of the line at the reference pressure p_0 (1 atm) and temperature T_0 (296 K) of the broadening gas (either air or CO_2), and χ is the ratio of the partial pressure of CO_2 to the total sample pressure in the cell. The temperature dependence exponents of air-broadened half width coefficients are n_a and the temperature dependent coefficient of air-induced shifts are δ'. In the present study, the rovibrational constants (G'-G'', B', H', D', B'', D'', H''), intensity parameters (band strengths and Herman-Wallis coefficients), self- and air-line mixing coefficients were fixed to the appropriate values reported in Refs. [21, 22], respectively, for the two bands. However, the individual air-broadened half width coefficients, air-induced pressure shift coefficients and their temperature dependences were adjusted. The resulting line parameters are listed in Tables 3 and 4 along with their uncertainties (described later). The line positions and intensities are the same as in Refs. [21, 22] and are shown here for identification and convenience for readers.

The final multispectrum fit for the region of the 30013←00001 band is shown in Fig. 1, where the observed line shapes are modeled with Speed Dependent Voigt profiles and asymmetric line mixing (off diagonal relaxation matrix). The bottom panel C displays all 39 experimental spectra. The other two panels demonstrate that proper weighting schemes are employed by showing the weighted observed-calculated residuals for B the 13 Kitt Peak room temperature spectra and A all 39 (room and cold) spectra. In Fig. 2 is a short spectral interval from Fig. 1 re-plotted to show in detail the 3 transitions, R16 to R20.

4. Theoretical Calculations

The half width coefficients of self-, O_2- and N_2-perturbed carbon dioxide were modeled using semiclassical calculations based on the real components of the Robert-Bonamy theory [28], (RRB). In this theoretical approach we can express the half width coefficient, γ, (which corresponds to b_L^0, used elsewhere in this article) of any given rovibrational transition f←i as the real part of the corresponding diagonal element of the complex relaxation matrix. In this semiclassical framework, the half width coefficients can be computed using the elements of the Liouville scattering matrix [29, 30]:

$$\gamma_{i \leftarrow f} = \frac{n_2}{2\pi c} \left\langle v \left[1 - e^{-{}^{R}S_2(f,i,J_2,v,b)} \right] \right\rangle_{v,b,J} \tag{7}$$

where n_2 is the number density of perturbers and $\langle\ \rangle_{v,b,J_2}$ is an average over all possible molecular trajectories of impact parameter b and initial relative velocity v, and the initial rotational quantum number J_2 of the collision partner. In (7), ${}^{R}S_2$ is real part of the second order term in the expansion of the scattering matrix. The size of the ${}^{R}S_2$ term depends on i) the rovibrational states involved in the transition and associated collision induced jumps from these energy level , ii) the intermolecular potential and iii) the collision dynamics. Present in (7) are the vibrational dephasing term, S_1, which appears only for transitions where there is a change in the vibrational state, and the imaginary part of the S_2 term. The potential leading to S_1 is written in terms of the isotropic induction and London dispersion interactions which depend on the vibrational dependence of the dipole moment and the polarizability of the radiating molecule. Since these parameters are not available for CO_2, the S_1 term has been omitted from the theoretical calculation. The effect of the imaginary part of S_2 will be investigated in a future study.

The intermolecular potential used in our calculations has both an electrostatic component (quadrupole moments of CO_2 with the quadrupole moment of N_2, O_2, or CO_2) and an atom-atom component based on parameters published by Rosenmann *et al.* [31]. The expression of Sack [32] expanded to the fourth order was used to express the atom-atom distance, r_{ij}, in terms of the center of mass separation, R. The Robert and Bonamy's second order in time approximation is used to describe the dynamics of the collisional processes.

All the molecular parameters for the CO_2-X (where X is N_2, O_2, or CO_2) systems used in the calculations are taken from the work of Rosenmann *et al.* [31]. The molecular trajectories are assumed to be curved (parabolic) rather than straight lines [28]. In this approximation the interaction potential is used to determine the distance, effective velocity, and force at closest approach. To simplify the trajectory calculations the isotropic part of the atom-atom expansion is approximated by a single isotropic Lennard-Jones 6-12 potential where the parameters are from Ref. 31. The reduced matrix elements of the radiating and perturbing molecules are evaluated using wavefunctions in the symmetric top basis and the energies are given in terms of the molecular rotational constants.

The calculation of N_2-, O_2-, and self-broadened half width coefficients were made for P-, Q-, and R-branch transitions of CO_2 for $|m|$ values from 1 to 121, where $m = -J''$ for P-branch transitions, $m = J''+1$ for R-branch transitions and $m = 0$ for the Q1 to Q121 transitions. The half width coefficients were calculated at 200 K, 250 K, 296 K, 300 K and 500 K by using the Gaussian method of moments to perform the averaging over the Maxwell-Boltzmann distribution of velocities. The air-broadened half width coefficients at each temperature were determined assuming binary collisions and Dalton's law of partial pressures

$$\gamma_{air} = 0.79 \times \gamma_{N_2} + 0.21 \times \gamma_{O_2} \qquad (8).$$

For atmospheric applications, both the temperature and pressure dependence of half width coefficients are required on a line-by-line basis. The temperature scaling law [33] can be used to determine the temperature dependence exponents, *n*, of the half width coefficient,

$$\gamma(T) = \gamma(T_0) \left\{ \frac{T_0}{T} \right\}^n . \qquad (9)$$

In recent years it has been shown that for some gas-perturber systems, such as for example foreign-broadened water, this scaling law does not apply [34-37]. However, as seen later, this does not seem to be the case for the present data.

The theoretical values of the temperature dependence exponents, *n*, were determined for each transition by a least-squares fits of *ln* [γ(T) / γ(T$_0$)] vs. *ln*[T$_o$/T] over the temperature range 200 to 500 K. We were also able to determine the error in the temperature dependence exponents using the half width values at any two of the five temperatures studied. This procedure provided ten 2-point temperature dependence exponents. The difference between each 2-point temperature dependence exponent and the 5-point fit value is calculated. The errors quoted in this work are the largest of these differences and believed to be more reliable than the statistical values taken from the fit. Table 5 gives the range of theoretical values for γ at 296 K and *n*.

5. Discussion of Results

We performed a number of comparisons in order to assess the quality of our retrieved broadening coefficients (air-broadened widths, pressure shifts and their temperature dependences). First, we noted that corresponding measurements for the two bands were in very close agreement for transitions with the same rotational quantum assignment (ΔJ, J″). This is demonstrated in Figs. 3 and 4 (panels A and C) where the air broadening measurements (widths, shifts and their temperature dependences) for 30012 ← 00001 and 30013 ← 00001 are plotted together as a function of m (where *m* = -*J″* for P branch lines and *J″*+1 for R branch lines). Also, for each *m* value we averaged the coefficients for transitions in the 30012 ← 00001 and 30013 ← 00001 vibrational bands. The percentage differences between the average and the individual measurements are displayed in panels B and D. For the air-broadened widths and pressure shifts in Fig. 3 A and C, the mean percentage differences were, respectively, +0.2(0.6) and +1(7), while for the temperature dependence coefficients of air-broadened widths and pressure shifts in Fig. 4 A and C, the mean percentage differences were, respectively, +0.05(2.27) and +1(10) The larger observed scatter in panels (B) and (D) of Figs. 3 and 4 for high values of $|m|$ was attributed to the weakness of the absorptions in the fitted data. As seen previously [e.g. 6, 21-24], the air-broadened half width coefficients have minimal vibrational dependence, whereas the air-induced shift coefficients in the 30012 ← 00001 band are slightly larger than those for the 30013 ← 00001 band.

Encouraged by the excellent agreement seen in Figs. 3 and 4, we averaged the pairs of observed values with the same rotational quantum assignment in the two bands. The values for all four types of broadening coefficients (widths, shifts and the temperature dependence of widths and shifts) are presented in Table 6, along with their respective percentage differences.

In Fig. 5, we compare the mean observed values from Table 6 and theoretically-predicted air broadened half width coefficients and their temperature dependences as a function of $|m|$. The error bars are plotted for the observed values, but these are usually smaller than the plot symbols. We note that P branch values are of even $|m|$ while R branch transitions are odd $|m|$, and we use open and solid plotting symbols to reveal if the coefficients also vary as a function of ΔJ. The corresponding theoretical air broadening widths and their temperature dependences are shown to $|m|$ =101 by solid curves in panel (A) for widths and (B) temperature dependence of widths. As shown in Fig. 5A, the observed air-broadened half width coefficients for the P and R branch transitions tend to lie on a smoothly changing curve that is below the calculated values for $|m| < 10$ and above them at higher $|m|$ values.

In contrast, in Fig. 5B, the temperature dependence of the widths for P and R branches do not fall on the same smoothly changing curve, and they are often different by more than the percent agreement in the average n. Normally, such differences would be attributed to experimental error since the observed widths do follow the trends predicted by theory. However, in the present study, two different bands are analyzed using the same spectral data, and as seen in Fig. 4, the observed differences in their temperature dependences are very similar at each m. In contrast, averaged temperature dependence in Fig. 5B is different from the calculation by larger amounts; the P and R branch lines also have slightly different observed values. One possibility is that some systematic error in comparison with the calculations was introduced in the retrievals because the temperature dependence of the line mixing could not be determined with the present dataset. Further investigation is needed to clarify this.

Nevertheless, both the measured widths and temperature dependence coefficients do fall reasonably close to the calculated values up to $|m| < 40$. The agreement between theory and empirical widths is best for $6 \leq m \leq 26$. Between $|m|$ = ~26 and = 55, the measured widths are lower than the calculated values. There are two important exceptions, however. The "kink" predicted for the low| *m*| widths is not observed at all, while for the temperature dependence of widths the local minimum at $|m| = 14$ is observed closer to $|m| = 18$.

Beyond the range of our empirical averages, the calculated widths and temperature dependences steadily decrease with increasing $|m|$, reaching widths of 0.055 cm^{-1} atm^{-1} at 296 K and n of 0.5 at $|m| = 101$. To match the calculated widths to the averaged measurements, a scaling factor of 0.96 was applied, and the resulting curve is shown by the dash-dot line in Fig. 5A. We feel that the best results for the scientific community are the averaged measured air-broadened half width coefficients for $|m|$ up to 50 (Table 6) and the scaled theoretical prediction above $|m| = 50$.

The recommendation for the temperature dependence of air-broadened widths is less clear. For the entire range of $|m|$ where measurements are available, the power law model fits the calculated studies fairly well. Indeed, for most applications, the power law gives a reasonable description of the temperature dependence of the air-broadened half width coefficients over the range T = 200-500 K. Depending on the requirements of atmospheric applications, the theoretical values might be sufficiently reliable. Measurements are needed to validate the theoretical model at higher J.

The temperature dependence coefficients, δ', for air-induced shifts vs. $|m|$ displayed in Fig. 4C represent the first measurements in any CO_2 band, but there is no obvious trend in the retrieved values of δ' with $|m|$ or vibrational band. We observe that within the scatter of the experimental data, most of the δ' coefficients are about -6×10^{-5} $cm^{-1}atm^{-1}K^{-1}$, and this is our recommended value for this coefficient.

The panels in Fig. 6 present the percentage differences between the retrieved air-broadened half width coefficients and similar data sets available in the literature, plotted for both the A) 30013 ← 00001 and B) 30012 ← 00001 bands as a function of *m*. The scatter in our percentage differences occur at very low or at very high *J* values, or in spectral regions where the lines overlap with hot band transitions. The present results agree best with the results from the room temperature study of Devi et al. [21] (also a constrained multispectrum analysis) and those of Predoi-Cross et al. [24] where the same type of line shape model was used. The differences between the present set of air-broadened half width coefficients and those of Toth et al. [6] or HITRAN 2004 [38] are largely due to the difference in value between the half width coefficients retrieved with a speed-dependent Voigt model with line mixing and those retrieved with the standard Voigt model.

The panels in Fig. 7 present the ratios between the retrieved air-induced pressure shift parameters and data sets available in the literature, plotted as a function of *m* for both the A) 30013 ← 00001 and B) 30012 ← 00001 bands. For $|m| > 40$ and at very low *m* values we can see that the air-pressure shift coefficients are different than those reported by Toth et al. [6] and Predoi-Cross et al. [24], but these are still in good agreement with those from the room temperature constrained analysis studies [21, 22].

6. Uncertainties

Ultimately, it is not the uncertainties in the half width and pressure shift parameters that are important, but the uncertainty in the half width and pressure shift at the temperature of the gas being simulated. When one uses a half width at 296 K and its temperature dependence exponent from a database such as the HITRAN, it is assumed that the half widths near 296 K are the best determined and the uncertainty in *n* increases the uncertainty in half width as the temperature is farther from 296 K. In fact, for each line the experimental values of the two half width parameters and of the two pressure shift parameters are highly correlated and the uncertainty as a function of temperature looks quite different.

$$\varepsilon_{b_L}^2 = \left(\frac{T_0}{T}\right)^{2n} \varepsilon_{b_L^0}^2 + \left[\mathrm{b_L}(T)\ln\left(\frac{T_0}{T}\right)\right]^2 \varepsilon_n^2 + 2\rho_{b_L^0 n}\mathrm{b_L}(T)\left(\frac{T_0}{T}\right)^n \ln\left(\frac{T_0}{T}\right)\varepsilon_{b_L^0}\varepsilon_n \qquad (10)$$

$$\varepsilon_\delta^2 = \varepsilon_{\delta^0}^2 + (T - T_0)^2 \varepsilon_{\delta'}^2 + 2\rho_{\delta^0\delta'}(T - T_0)\varepsilon_{\delta^0}\varepsilon_{\delta'} \qquad (11)$$

In these expressions, ε is the uncertainty in the parameter in the subscript and ρ is the correlation between the two parameters in the subscript. Tables 3 and 4 list these correlations ($\rho_{b\text{-}n}$ and $\rho_{\delta^0\delta'}$) for each spectral line.

Figure 8A displays the formal uncertainty in the air-broadened Lorentz half width for each spectral line from P2 to P42 as a function of temperature for the 30013 ← 00001 band measured in this study. The uncertainties in half width coefficients for the low *J* lines are relatively constant over the range of temperature of the spectra in the fit, namely 215 to 294

K. For higher *J* lines, the strengths of the lines become small enough at lower temperatures that the fit does not constrain the half widths at those temperatures and the temperature region in which the half widths are best determined narrows to only the higher temperatures. Figure 8B displays the minimum half width uncertainty as a function of temperature for each of the same spectral lines in Fig. 8A. The trend toward higher temperature at higher rotational quantum numbers is clear as is the trend toward lower uncertainties in the strongest lines at the intermediate *Js*. Figure 9 shows the corresponding effects in the pressure shift parameters. The minimum uncertainties are generally a bit smaller and occur at temperatures 2 to 5 K warmer than those of the half widths. The small irregularity for P18 observed in Fig. 9B is due to a problem with a hot band line blended with P18 that was not modeled as well as possible. Most of the irregularities in Fig. 8A, on the other hand, are due to a small round-off problem in the fitting software's uncertainty analysis for Lorentz widths.

The uncertainties derived from the fits for both the Lorentz width and pressure shift parameters are smaller than the real uncertainties. Due to the large quantity of data within the solution, the uncertainty due to the noise levels of the spectra is very small. At this level there are various other problems with the fits that dominate the actual uncertainties. These include uncertainties in the measurement of the physical conditions of the gas, uncertainties in the spectral line shapes and some modeling of the spectral line parameters used. In particular, there was no effort to model either line mixing or speed dependence as a function of temperature. Each has only a small effect upon the solution in the first place. While the speed dependence model represents all temperatures, the model is unlikely to hold rigorously for all collisional speeds. In the comparisons between the two bands, the half widths and pressure shifts differ by a few times the formal uncertainties. For the half widths the differences between the two bands seem to be random as a function of rotational quantum number, so it is unlikely that these differences are due to vibrational effects in carbon dioxide, but rather due to some systematic problem in the fits. The general shape of the uncertainty with temperature is independent of these systematic effects and the relative uncertainty from temperature to temperature is close to that shown in Figs. 8 and 9.

Combination of widths and shifts at 296 K with temperature dependence parameters determined from an unrelated study do not profit from the correlations displayed here. The smallest uncertainty becomes that at 296 K and the uncertainty in n causes them to rise as the temperature moves farther from that temperature. In order to get high quality Lorentz half widths and pressure shifts requires that they be determined in the same study with their temperature dependences.

7. Conclusions

We confirmed earlier measurements of air-broadened Lorentz half widths and air-induced pressure shifts [21-24] and determined extensive temperature dependence values up to $J'' = 45$ simultaneously for two near-IR bands of $^{12}CO_2$ (30012←00001 at 6348 cm^{-1} and 30013←00001 at 6228 cm^{-1}). The broadening parameters were retrieved to using constrained multispectrum nonlinear least squares curve fitting employing speed dependent Voigt profiles and relaxation matrix line mixing. This procedure was applied to high resolution spectra (37 air-broadened CO_2 and two of pure CO_2) recorded at temperatures between 215 and 294 K using two different Fourier transform spectrometers. We performed semiclassical theoretical calculations using the Robert-Bonamy formalism [28] and found small differences (< 4%) between the measured and calculated air-broadened half width coefficients and the corresponding temperature dependence coefficients. We observed no obvious vibrational dependence for the temperature dependence of air-broadened widths of CO_2. The measured temperature dependences of the air-induced pressure shifts revealed no dependence on the rotational quantum numbers; therefore an average value of -6.0×10^{-5} $cm^{-1}atm^{-1}K^{-1}$ was recommended for atmospheric calculations.

Acknowledgements

A. Predoi-Cross and A.R.W. Mckellar are grateful for financial support from the National Sciences and Engineering Research Council of Canada (NSERC). The research at the Jet Propulsion laboratory (JPL), California Institute of Technology, was performed under contract with National Aeronautics and Space Administration. The support received from the National Science Foundation under Grant No. ATM-0338475 to the College of William and Mary is greatly appreciated. R.R. Gamache is pleased to acknowledge support of this research by the National Science Foundation through Grant No. ATM-0803135. The authors thank Mike Dulick of the National Solar Observatory for his assistance in obtaining the data recorded at Kitt Peak.

References

1. H.H. Aumann, D. Gregorich, and S. Gaiser. Geophys. Res. Lett. **32**, **L05806** (2005). doi:10.1029/2004GL021784.
2. D. Diebel, M. Langevin, D. Klaes, P. Courtier, T. Phuloin, F. Cayla, and G. Chalon. Proceedings of the EUMETSAT User Conference, Septembre 1997. EUMETSAT.
3. D. Crisp, R.M. Atlas, F.M. Breon, L.R. Brown, J.P. Burrows, P. Ciais, B.J. Connor, S.D. Doney, I.Y. Fung, D.J. Jacob, C.E. Miller, D. O'Brien, S. Pawson, J.T. Randerson, P. Rayner, R.J. Salawitch, S.P. Sander, B. Sen, G.L. Stephens, P.P. Tans, G.C. Toon, P.O. Wennberg, S.C. Wofsy, Y.L. Yung, Z. Kuang, B. Chudasama, G. Sprague, B. Weiss, R. Pollock, D. Kenyon, and S. Schroll. Adv. Space Res. **34**, (2004) 700.
4. T. Hamazaki, Y. Kaneko, A. Kuze, and K. Kondo. SPIE, **5659**, 73 (2005).
5. L.S. Rothman, R.L. Hawkins, R.B. Wattson, and R.R. Gamache. J. Quant. Spectrosc. Radiat. Transfer, **48**, 537 (1992).
6. R.A. Toth, C.E. Miller, V. M. Devi, D.C. Benner, and L.R. Brown. J. Mol. Spectrosc. **246**, 133 (2007).
7. K.I. Arshinov and N.S. Leshenyuk. Quant. Electron. **27**, 503 (1997).
8. A.F. Aushev, N.F. Borisova, E.S. Bykova, V.M. Osipov, and V.V. Tsukanov. Opt. Spectrosc. (USSR) **68**, 700 (1990).
9. R.A. Brownsword, J.S. Salh, and I.W.M. Smith. J. Chem. Soc. Faraday Trans. **93**,191 (1995).
10. L. Rosenmann, M.Y. Perrin, and J. Taine. J. Chem. Phys. **88**, 2995 (1988).
11. L. Rosenmann, M.Y. Perrin, J.M. Hartmann, and J. Taine. J. Quant. Spectrosc. Radiat. Transfer, **40**, 569 (1988).
12. M. Margottin-Maclou, P. Dahoo, A. Henry, A. Valentin, and L. Henry. J. Mol. Spectrosc. **131**, 21 (1988).
13. W.G. Planet, G.L. Tettemer, and J.S. Knoll. J. Quant. Spectrosc. Radiat. Transfer, **20**, 547 (1978).
14. R.S. Eng and A. W. Mantz. J. Mol. Spectrosc. **74**, 331(1979).
15. G.L. Tettemer and W.G. Planet. J. Quant. Spectrosc. Radiat. Transfer, **24**, 343 (1980).
16. V.M. Devi, B. Fridovich, G.D. Jones, and D.G.S. Snyder. J. Mol. Spectrosc. **105**, 61(1984).
17. C. Cousin, R. Le Doucen, J.P. Houdeau, C. Boulet, and A. Henry. Appl. Opt. **25**, 2434 (1986).

18. P. Varanasi. J. Quant. Spectrosc. Radiat. Transfer, **39**, 13 (1988).
19. F.P.J. Valero and C.B. Suarez. J. Quant. Spectrosc. Radiat. Transfer, **19**, 579 (1978).
20. C.B. Suarez and F.P.J. Valero. J. Mol. Spectrosc. **71**, 46 (1978).
21. V.M. Devi, D.C. Benner, L.R. Brown, C.E. Miller, and R.A. Toth. J. Mol. Spectrosc. **242**, 90 (2007).
22. V.M. Devi, D.C. Benner, L.R. Brown, C.E. Miller, and R.A. Toth. J. Mol. Spectrosc. **245**, 52 (2007).
23. A. Predoi-Cross, A.V. Unni, W. Liu, I. Schofield, C. Holladay, A.R.W. McKellar, and D. Hurtmans. J. Mol. Spectrosc. **245**, 34 (2007).
24. A. Predoi-Cross, W. Liu, C. Holladay, A.V. Unni, I. Schofield, A.R.W. McKellar, and D. Hurtmans. J. Mol. Spectrosc. **246**, 98 (2007).
25. A. Levy, N. Lacome, and C. Chackerian Jr., Collisional line mixing, in: K.N. Rao, A.Weber (Eds.), Spectroscopy of the Earth's Atmosphere and Interstellar medium, Academic Press. Boston, MA, 1992, pp.261, Ch.2.
26. R.A. Toth, L.R. Brown, C.E. Miller, V.M. Devi, and D.C. Benner. J. Mol. Spectrosc. **239**, 221 (2006).
27. D.C. Benner, C.P. Rinsland, V.M. Devi, M.A.H. Smith, and D. Atkins. J. Quant. Spectrosc. Radiat. Transfer **53**, 705 (1995).
28. D. Robert and J. Bonamy. Journal de Physique, **20**, 923 (1979).
29. M. Baranger. Phys Rev. **112**, 855 (1958).
30. A. Ben-Reuven. Adv. Chem. Phys., I. Prigogine and S.A. Rice Editors, Academic Press, New York. p. 235 (1975).
31. L. Rosenmann, J.-M. Hartmann, M.Y. Perrin, and J. Taine. J Chem Phys. **88**, 2999 (1988).
32. R.A. Sack. J. Math. Phys. **5**, 260 (1964).
33. G. Birnbaum. Advances in Chem. Phys. **12**, 487 (1967).
34. G. Wagner, M. Birk, R.R. Gamache, and J.-M. Hartmann. J. Quant. Spectrosc. Radiat. Transfer **92**, 211 (2005).
35. R.A. Toth, L.R. Brown, M.A.H. Smith, V.M. Devi, D.C. Benner, and M. Dulick, J. Quant. Spectrosc. Radiat. Transfer **101**, 339 (2006).
36. B.K. Antony, S. Neshyba, and R.R. Gamache. J. Quant. Spectrosc. Radiat. Transfer, **105**, 148 (2006).

37. J.-M. Hartmann, J. Taine, J. Bonamy, B. Labani, and D. Robert. J. Chem. Phys. **86**, 144 (1987).

38. L.S. Rothman, D. Jacquemart, A. Barbe, D.C. Benner, M. Birk, L.R. Brown, M.R. Carleer, C. Chackerian, K. Chance, L.H. Coudert, V. Dana, V.M. Devi, J.M. Flaud, R.R. Gamache, A. Goldman, J.M. Hartmann, K.W. Jucks, A.G. Maki, J.Y. Mandin, S.T. Massie, J. Orphal, A. Perrin, C.P. Rinsland, M.A.H. Smith, J. Tennyson, R.N. Tolchenov, R.A. Toth, J. Vander Auwera, P. Varanasi, and G. Wagner. J. Quant. Spectrosc. Radiat. Transfer, **96**, 139 (2005).

LIST OF FIGURES

Figure 1. Multispectrum fit of all 39 spectra in the 6120-6280 cm^{-1} region of $^{12}C^{16}O_2$ (30013 ← 00001 and all other bands appearing in the fitted interval) using a Voigt profile modified with speed dependence and line mixing via relaxation matrix. (A) Weighted fit residuals (observed minus calculated on an expanded scale) from all spectra (B) Weighted fit residuals for the 13 room temperature spectra recorded at Kitt Peak and included in (A). (C) The 39 experimental spectra. The different colors correspond to various gas sample temperatures (black=room temperature Kitt Peak spectra, all other data are from NRC: red (296 K), light green (274 K), blue (259 K), dark. green (244 K), Cyan (234 K), pink (219 K) and dark Cyan (215 K).

Figure 2. An expanded portion from **Fig. 1** illustrating the multispectrum fit for R16 to R20 transitions of the 30013 ← 00001 band. (A) Weighted fit residual for all 39 spectra (B) Weighted fit residual for the 13 Kitt Peak room temperature spectra. (C) The 39 experimental spectra.

Figure 3. Experimental air-broadening coefficients for the 30013←00001 and 30012←00001 bands of $^{12}C^{16}O_2$ retrieved using constrained multispectrum fits. The horizontal axis is m, equal to $-J''$ for P branch lines and $J''+1$ for R branch lines. (A) Half width coefficients (B) Percentage differences of averaged half width coefficients from corresponding values in the 30012←00001 band. (C) Pressure-shift coefficients. (D) Percentage differences of averaged air-induced shift coefficients to corresponding values in the 30012←00001 band. For simplicity, the percentage differences in (B) and (D) are computed using coefficients from 30012←00001 band because the values for the other band give only mirror images.

Figure 4. Similar to Fig. 3, the temperature dependence exponents for air broadening coefficients for the 30013←00001 and 30012←00001 bands of $^{12}C^{16}O_2$ retrieved using constrained multispectrum fits. (A) n for half widths (B) Percentage differences from averaged n minus 30012←00001 values (C) Temperature dependent coefficients (δ') of air-induced shift coefficients (D) Percentage differences from averaged δ' minus 30012←00001 measurements.

Figure 5. Observed air-broadened half width coefficients of P and R branches of 30013←00001 and 30012←00001 of $^{12}CO_2$ compared to theoretical predictions. The horizontal axis is |*m*|, equal to *J*″ for P branch lines and *J*″+1 for R branch lines. (A) Averaged measured half widths from Table 6 (open and solid squares) with calculated values (solid line). The dash-dot-dash line shows the values recommended for atmospheric uses obtained by the combining observed values (for |*m*| =1-51) with calculated values (scaled by 0.96) for |*m*| = 52-101 (see text for details). (B) Averaged temperature dependence exponents (*n*) of air-broadened half width coefficients for the P and R branches with the theoretical prediction (solid line). The horizontal dashed curve corresponds to the commonly used default value of *n* = 0.75.

Figure 6. Percent differences between present air-broadened widths and other reported measurements (PW – others)/PW×100 for transitions in the A) 30013←00001 band and B) 30012←00001 bands. All values are plotted as a function of the *m* value. The mean and standard deviation for each set of % differences are given in the legend.

Figure 7. Ratios of present air-broadened pressure shifts to other reported measurements for transitions in the A) the 30013←00001 band and B) the 30012←00001 band. The data are plotted as a function of *m*. The mean and standard deviation for each set of ratios are given in the legend.

Figure 8 A) The uncertainty of air-broadened widths as a function of temperature for 30013 ← 00001 with B) the corresponding minimum uncertainty where the plot symbol is equal to the lower state *J*. Traces for P10 through P32 overlap extensively and are not labeled individually.

Figure 9. A) The uncertainty of air-broadened pressure-induced shifts as a function of temperature for 30013 ← 00001 with B) the corresponding minimum uncertainty where the plot symbol is equal to the lower state *J*. Traces for P10 through P26 overlap extensively and are not labeled individually.

LIST OF TABLES

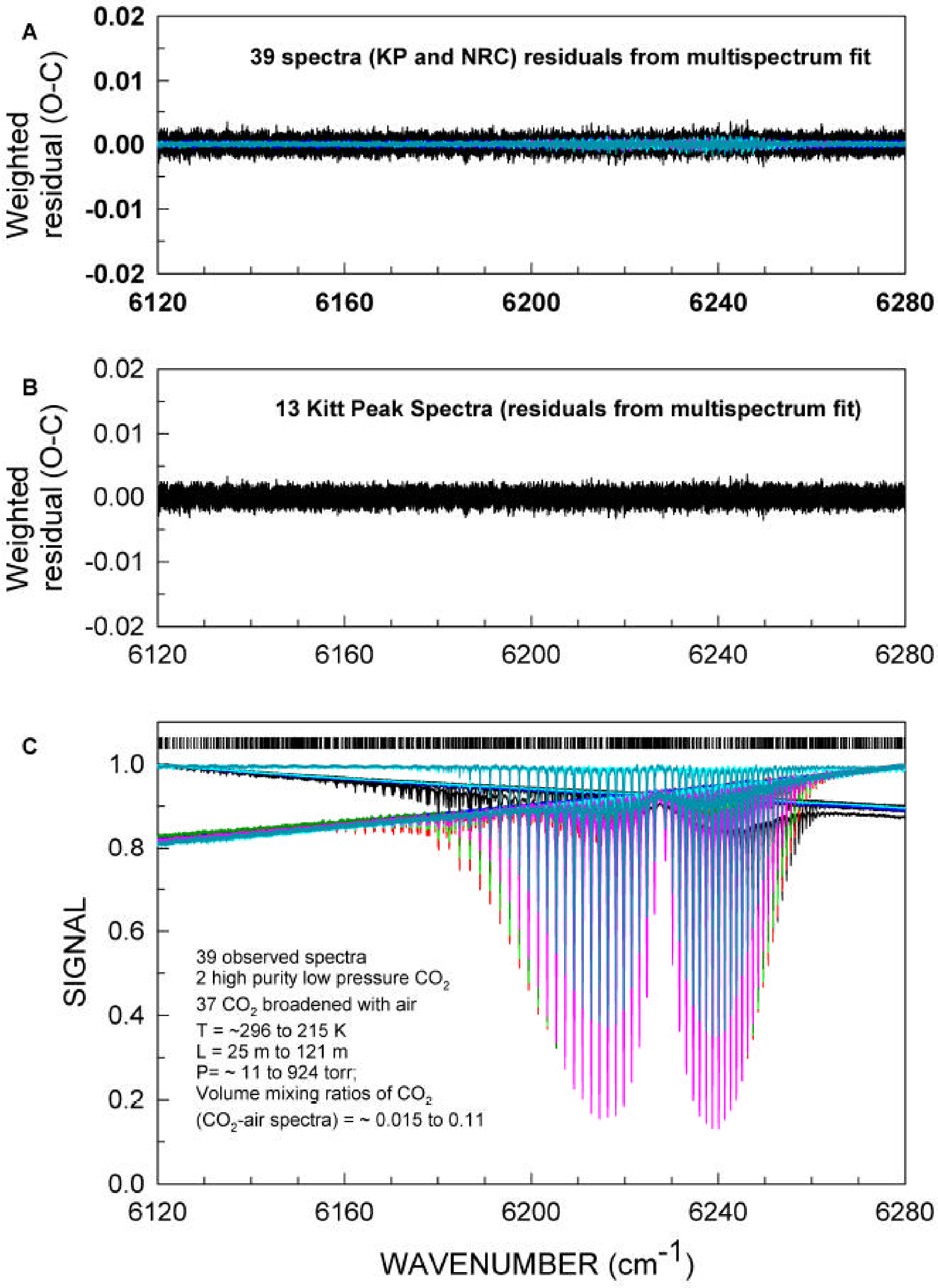
A
39 spectra (KP and NRC) residuals from multispectrum fit
Weighted residual (O-C)
0.02
0.01
0.00
-0.01
-0.02
6120
6160
6200
6240
6280
B
13 Kitt Peak Spectra (residuals from multispectrum fit)
Weighted residual (O-C)
0.02
0.01
0.00
-0.01
-0.02
6120
6160
6200
6240
6280
C
SIGNAL
1.0
0.8
0.6
0.4
0.2
0.0
39 observed spectra
2 high purity low pressure CO_2
37 CO_2 broadened with air
T = ~296 to 215 K
L = 25 m to 121 m
P= ~ 11 to 924 torr;
Volume mixing ratios of CO_2
(CO_2-air spectra) = ~ 0.015 to 0.11
6120
6160
6200
6240
6280
WAVENUMBER (cm^{-1})

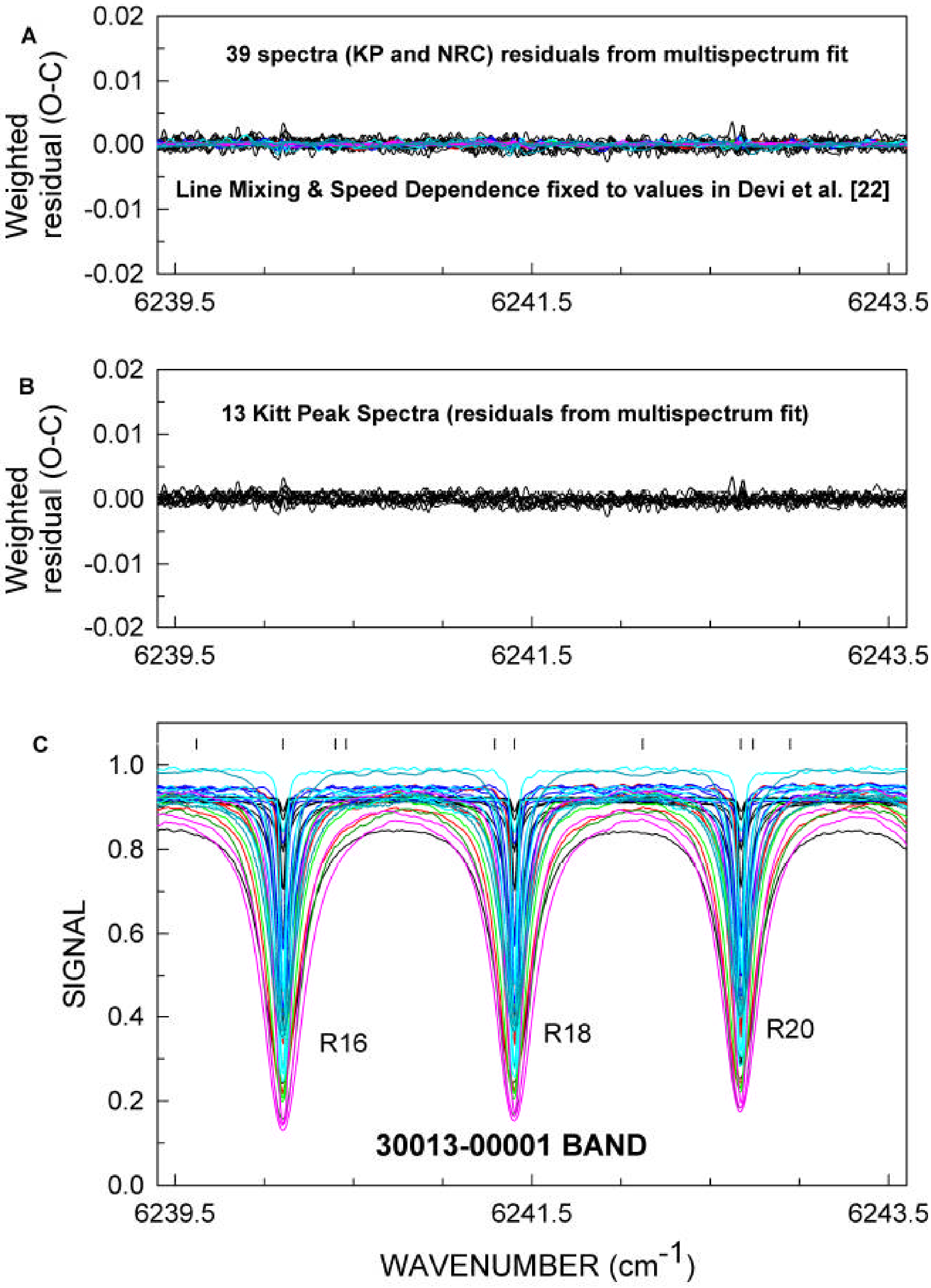
A
39 spectra (KP and NRC) residuals from multispectrum fit
Line Mixing & Speed Dependence fixed to values in Devi et al. [22]
Weighted residual (O-C)
0.02
0.01
0.00
-0.01
-0.02
6239.5
6241.5
6243.5
B
13 Kitt Peak Spectra (residuals from multispectrum fit)
Weighted residual (O-C)
0.02
0.01
0.00
-0.01
-0.02
6239.5
6241.5
6243.5
C
SIGNAL
1.0
0.8
0.6
0.4
0.2
0.0
R16
R18
R20
30013-00001 BAND
6239.5
6241.5
6243.5
WAVENUMBER (cm^{-1})

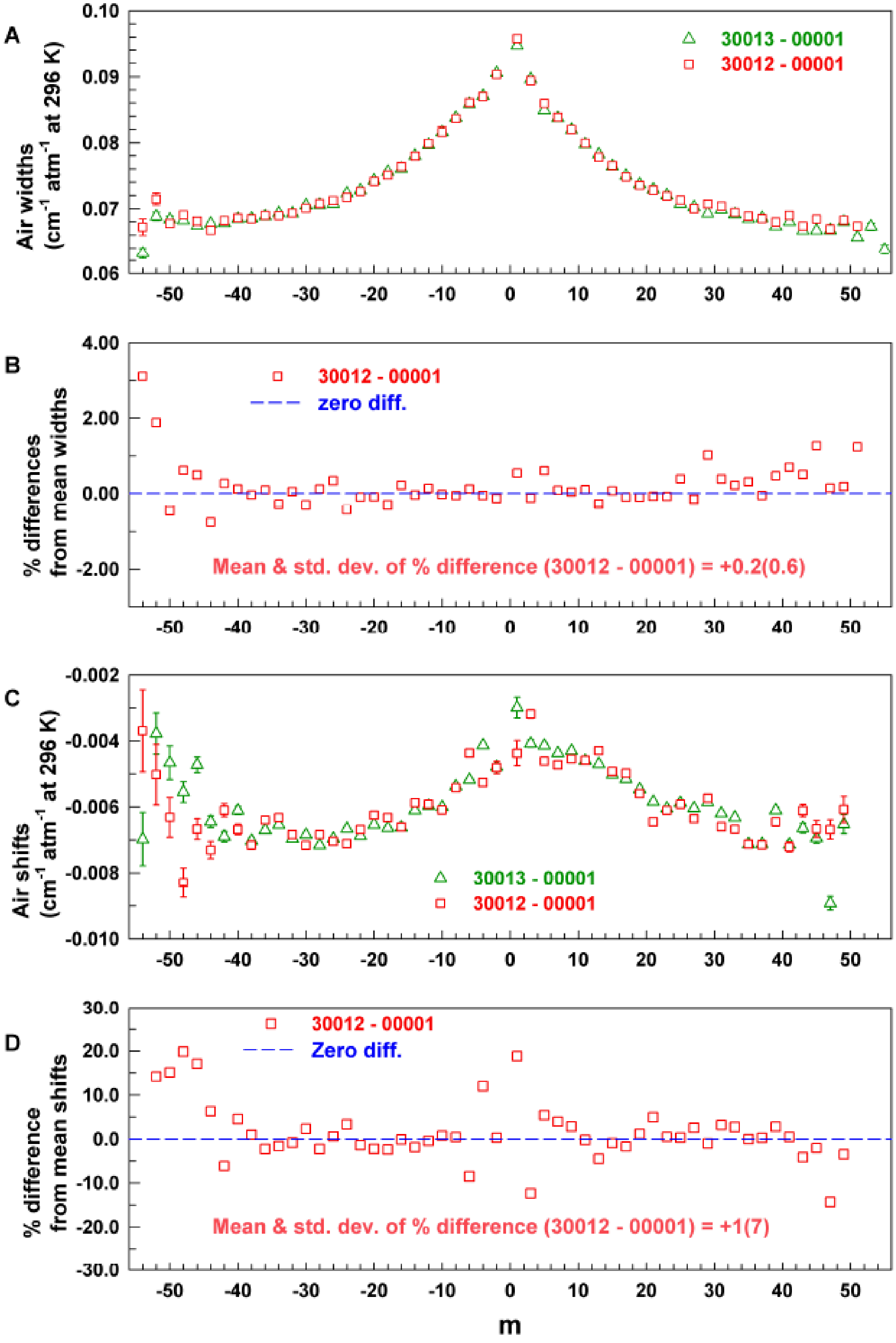
A
Air widths
(cm^{-1} atm^{-1} at 296 K)
0.10
0.09
0.08
0.07
0.06
-50
-40
-30
-20
-10
0
10
20
30
40
50
30013 - 00001
30012 - 00001
B
% differences
from mean widths
4.00
2.00
0.00
-2.00
30012 - 00001
zero diff.
Mean & std. dev. of % difference (30012 - 00001) = +0.2(0.6)
C
Air shifts
(cm^{-1} atm^{-1} at 296 K)
-0.002
-0.004
-0.006
-0.008
-0.010
30013 - 00001
30012 - 00001
D
% difference
from mean shifts
30.0
20.0
10.0
0.0
-10.0
-20.0
-30.0
30012 - 00001
Zero diff.
Mean & std. dev. of % difference (30012 - 00001) = +1(7)
m

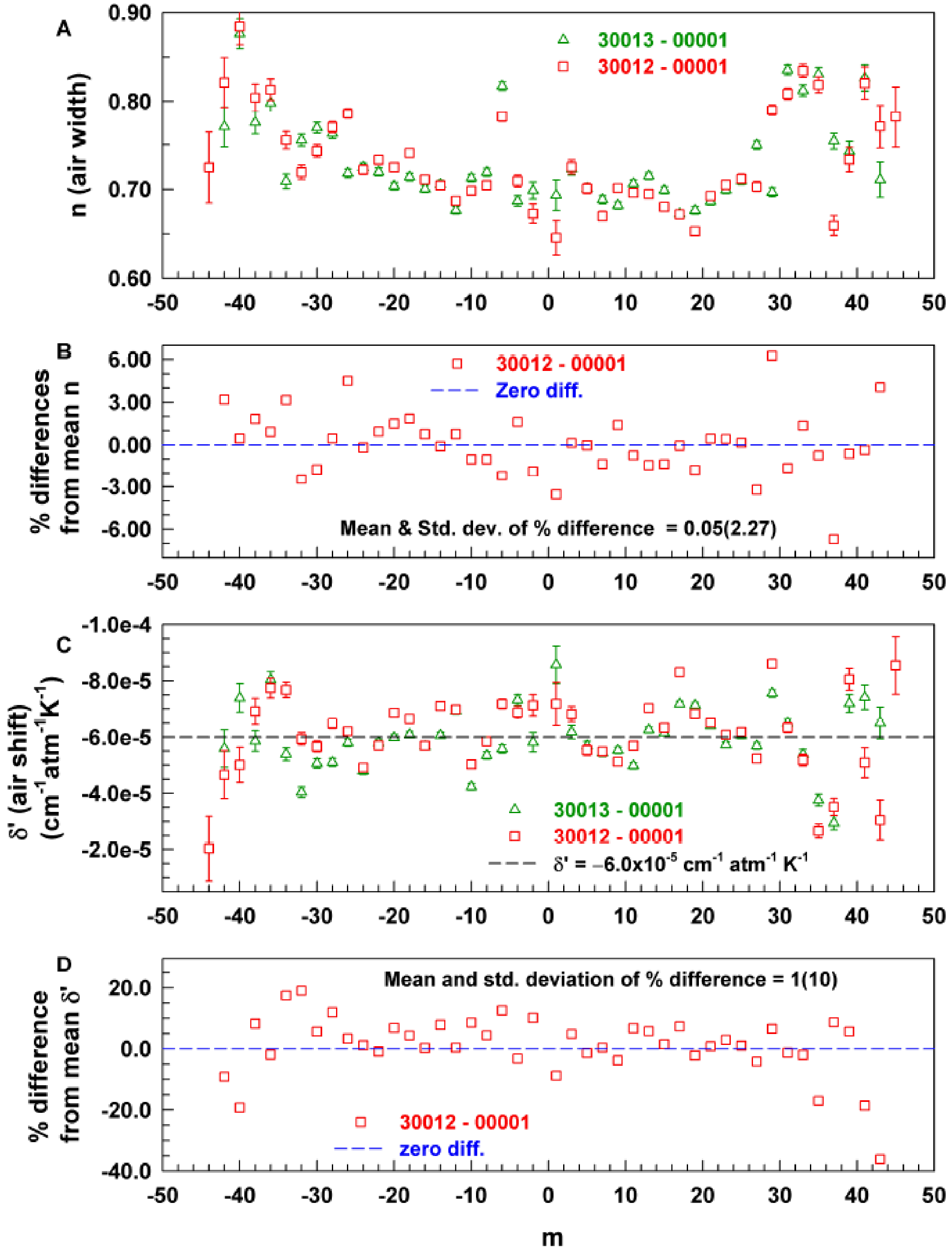
A
n (air width)
0.90
0.80
0.70
0.60
30013 - 00001
30012 - 00001
-50
-40
-30
-20
-10
0
10
20
30
40
50
B
% differences from mean n
6.00
3.00
0.00
-3.00
-6.00
30012 - 00001
Zero diff.
Mean & Std. dev. of % difference = 0.05(2.27)
C
δ' (air shift) (cm^{-1}atm^{-1}K^{-1})
-1.0e-4
-8.0e-5
-6.0e-5
-4.0e-5
-2.0e-5
30013 - 00001
30012 - 00001
δ' = –6.0x10^{-5} cm^{-1} atm^{-1} K^{-1}
D
% difference from mean δ'
20.0
0.0
-20.0
-40.0
Mean and std. deviation of % difference = 1(10)
30012 - 00001
zero diff.
m

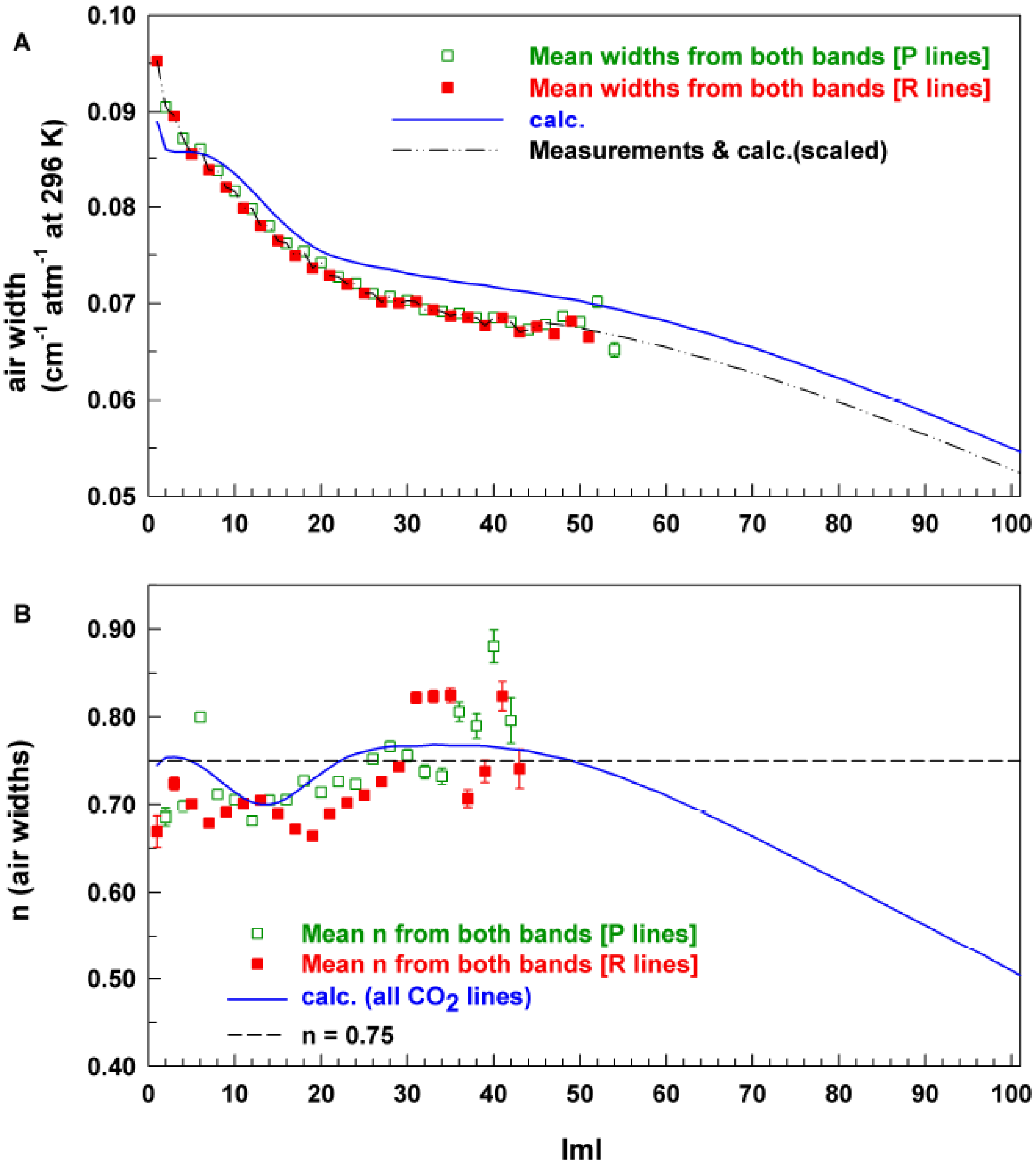
A
0.10
0.09
0.08
0.07
0.06
0.05
air width
(cm^{-1} atm^{-1} at 296 K)
Mean widths from both bands [P lines]
Mean widths from both bands [R lines]
calc.
Measurements & calc.(scaled)
0
10
20
30
40
50
60
70
80
90
100
B
0.90
0.80
0.70
0.60
0.50
0.40
n (air widths)
Mean n from both bands [P lines]
Mean n from both bands [R lines]
calc. (all CO$_2$ lines)
n = 0.75
lml

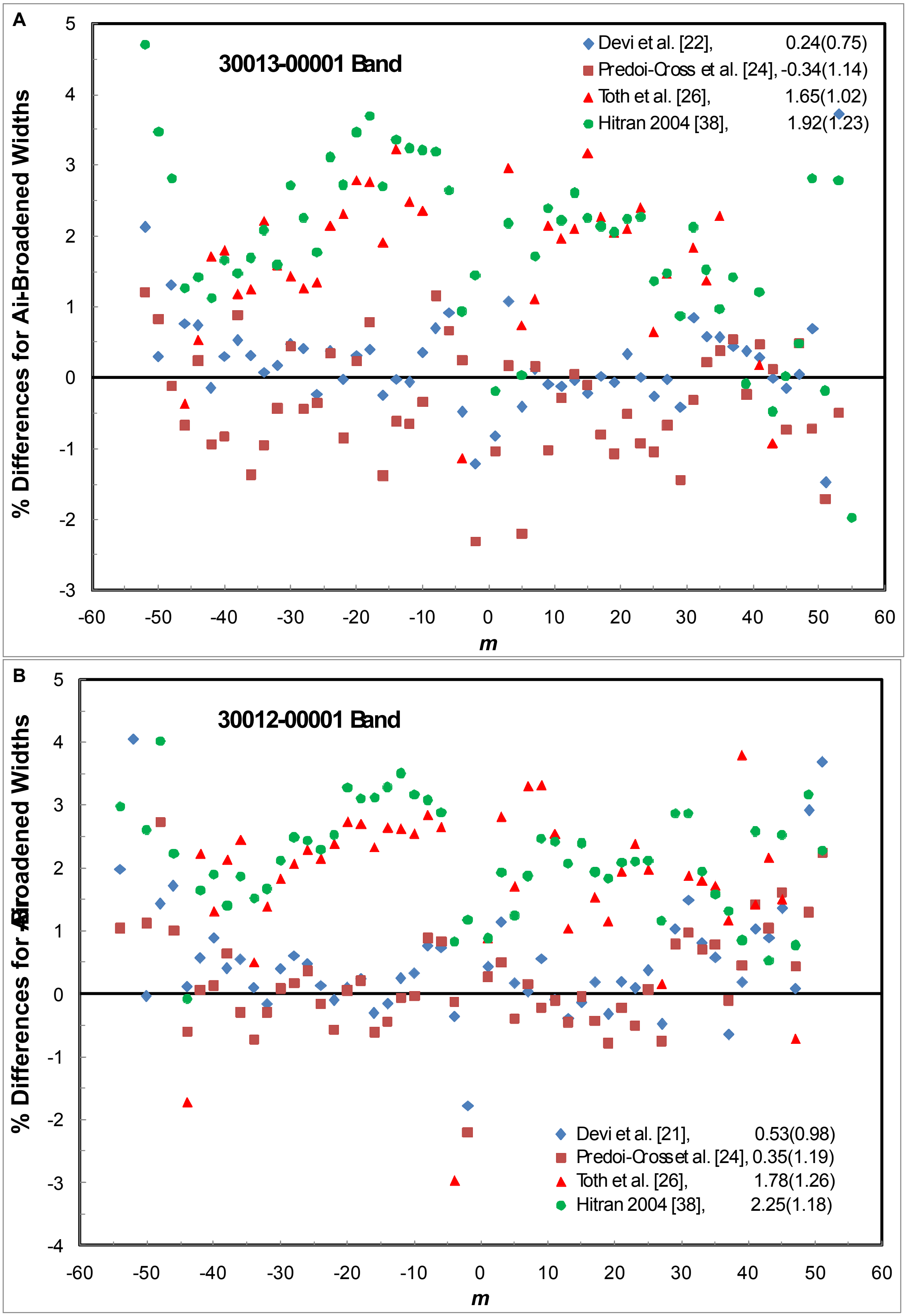
A
30013-00001 Band
Devi et al. [22], 0.24(0.75)
Predoi-Cross et al. [24], -0.34(1.14)
Toth et al. [26], 1.65(1.02)
Hitran 2004 [38], 1.92(1.23)
% Differences for Ai-Broadened Widths
5
4
3
2
1
0
-1
-2
-3
-60
-50
-40
-30
-20
-10
0
10
20
30
40
50
60
m
B
30012-00001 Band
Devi et al. [21], 0.53(0.98)
Predoi-Cross et al. [24], 0.35(1.19)
Toth et al. [26], 1.78(1.26)
Hitran 2004 [38], 2.25(1.18)
% Differences for Air-Broadened Widths
5
4
3
2
1
0
-1
-2
-3
-4
-60
-50
-40
-30
-20
-10
0
10
20
30
40
50
60
m

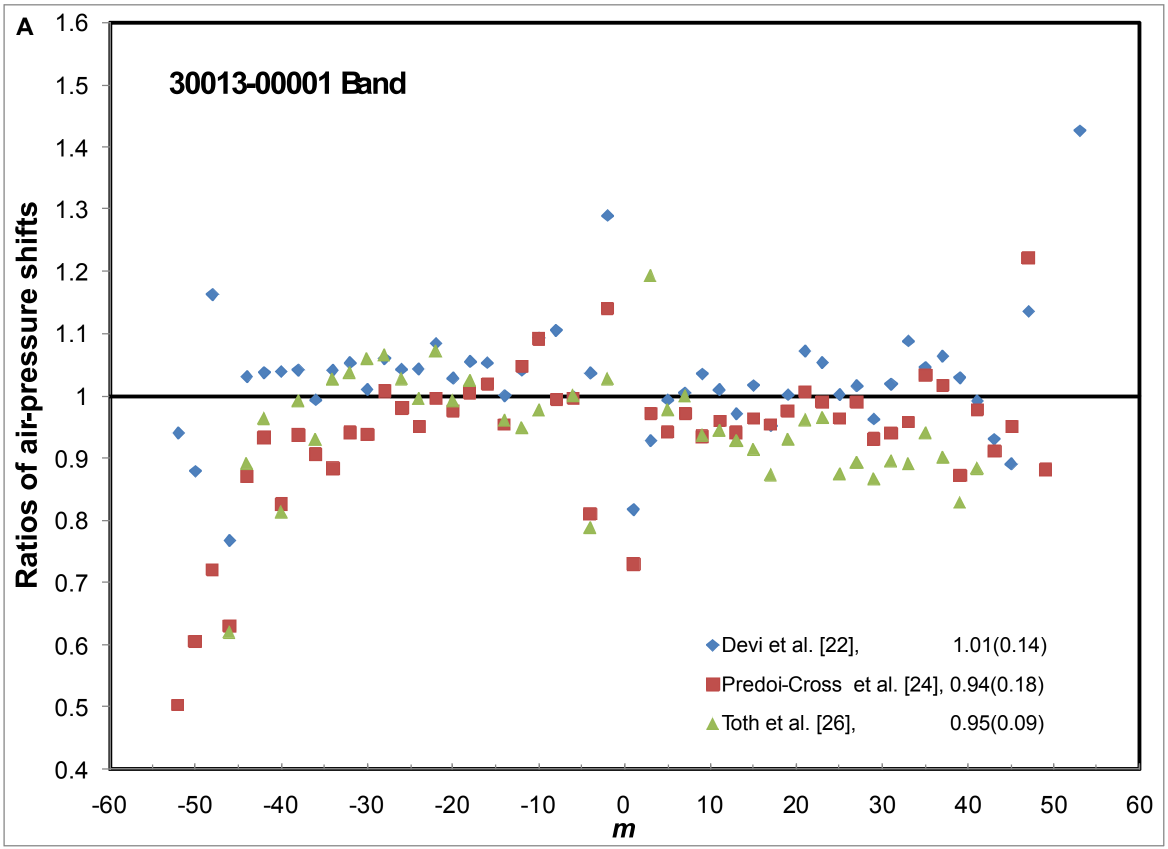
A
30013-00001 Band
Ratios of air-pressure shifts
1.6
1.5
1.4
1.3
1.2
1.1
1
0.9
0.8
0.7
0.6
0.5
0.4
-60
-50
-40
-30
-20
-10
0
10
20
30
40
50
60
m
◆ Devi et al. [22], 1.01(0.14)
■ Predoi-Cross et al. [24], 0.94(0.18)
▲ Toth et al. [26], 0.95(0.09)

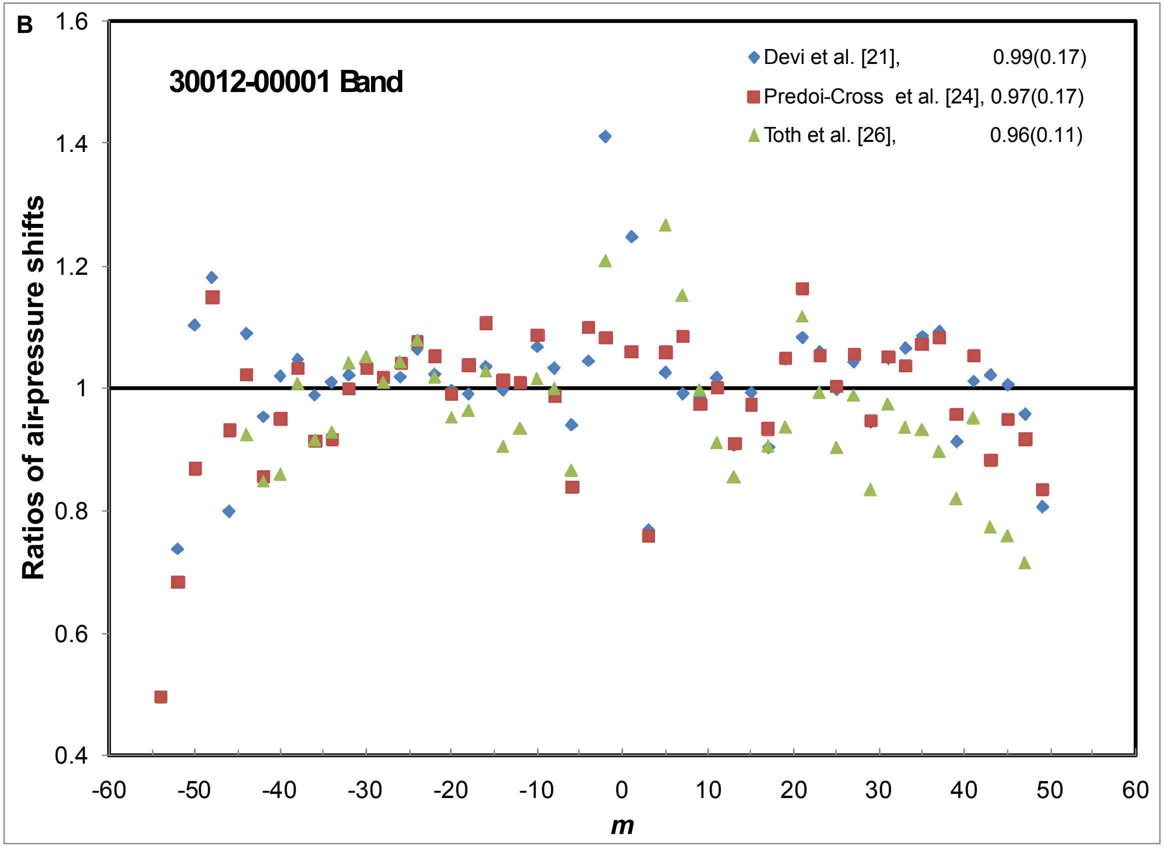
B
30012-00001 Band
Ratios of air-pressure shifts
1.6
1.4
1.2
1
0.8
0.6
0.4
-60
-50
-40
-30
-20
-10
0
10
20
30
40
50
60
m
◆ Devi et al. [21], 0.99(0.17)
■ Predoi-Cross et al. [24], 0.97(0.17)
▲ Toth et al. [26], 0.96(0.11)

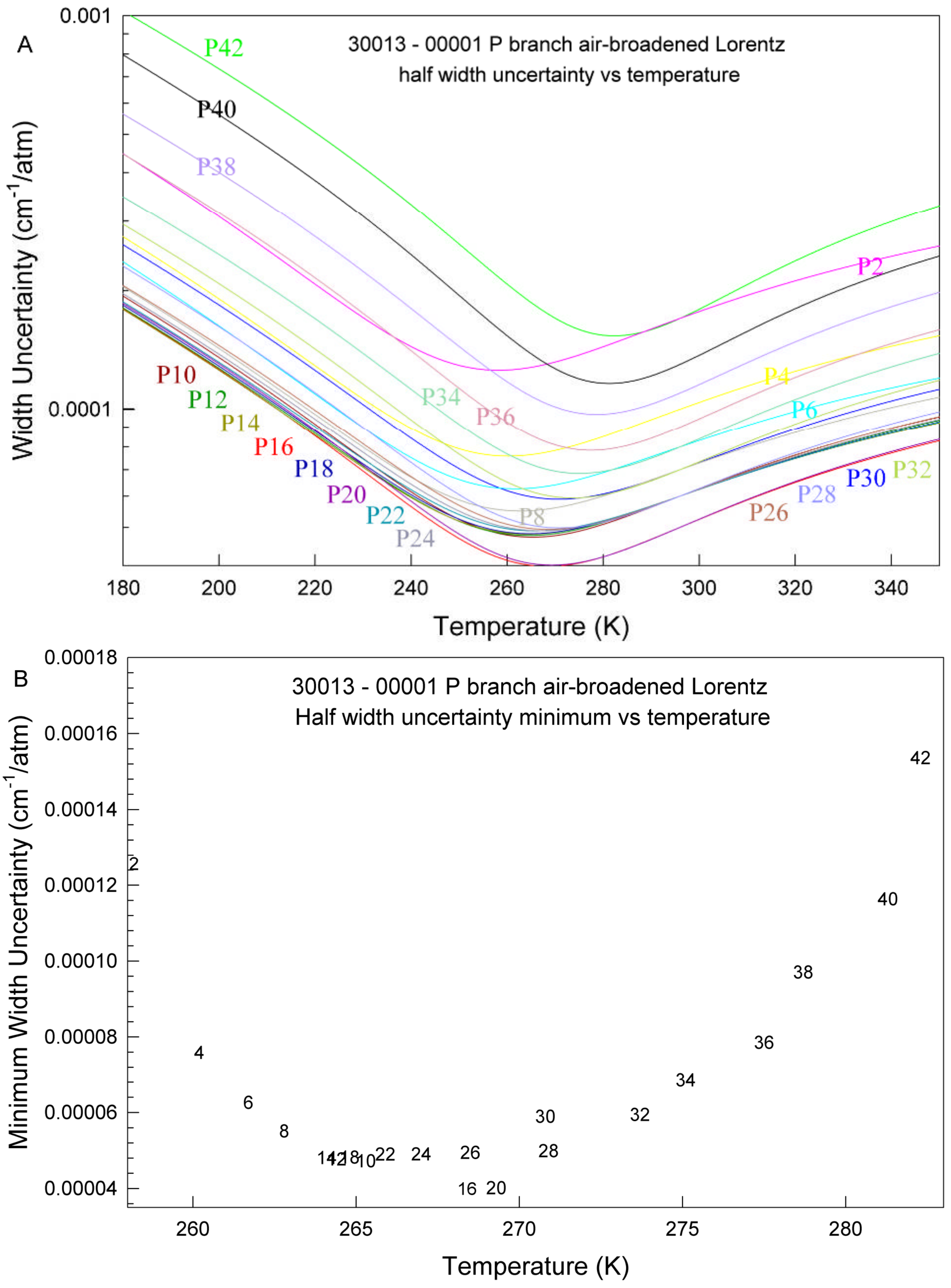
A
30013 - 00001 P branch air-broadened Lorentz
half width uncertainty vs temperature
Width Uncertainty (cm^{-1}/atm)
0.001
0.0001
Temperature (K)
180
200
220
240
260
280
300
320
340
P42
P40
P38
P2
P4
P6
P34
P36
P8
P10
P12
P14
P16
P18
P20
P22
P24
P26
P28
P30
P32
B
30013 - 00001 P branch air-broadened Lorentz
Half width uncertainty minimum vs temperature
Minimum Width Uncertainty (cm^{-1}/atm)
0.00018
0.00016
0.00014
0.00012
0.00010
0.00008
0.00006
0.00004
Temperature (K)
260
265
270
275
280
2
4
6
8
14
12
18
10
22
24
26
16
20
28
30
32
34
36
38
40
42

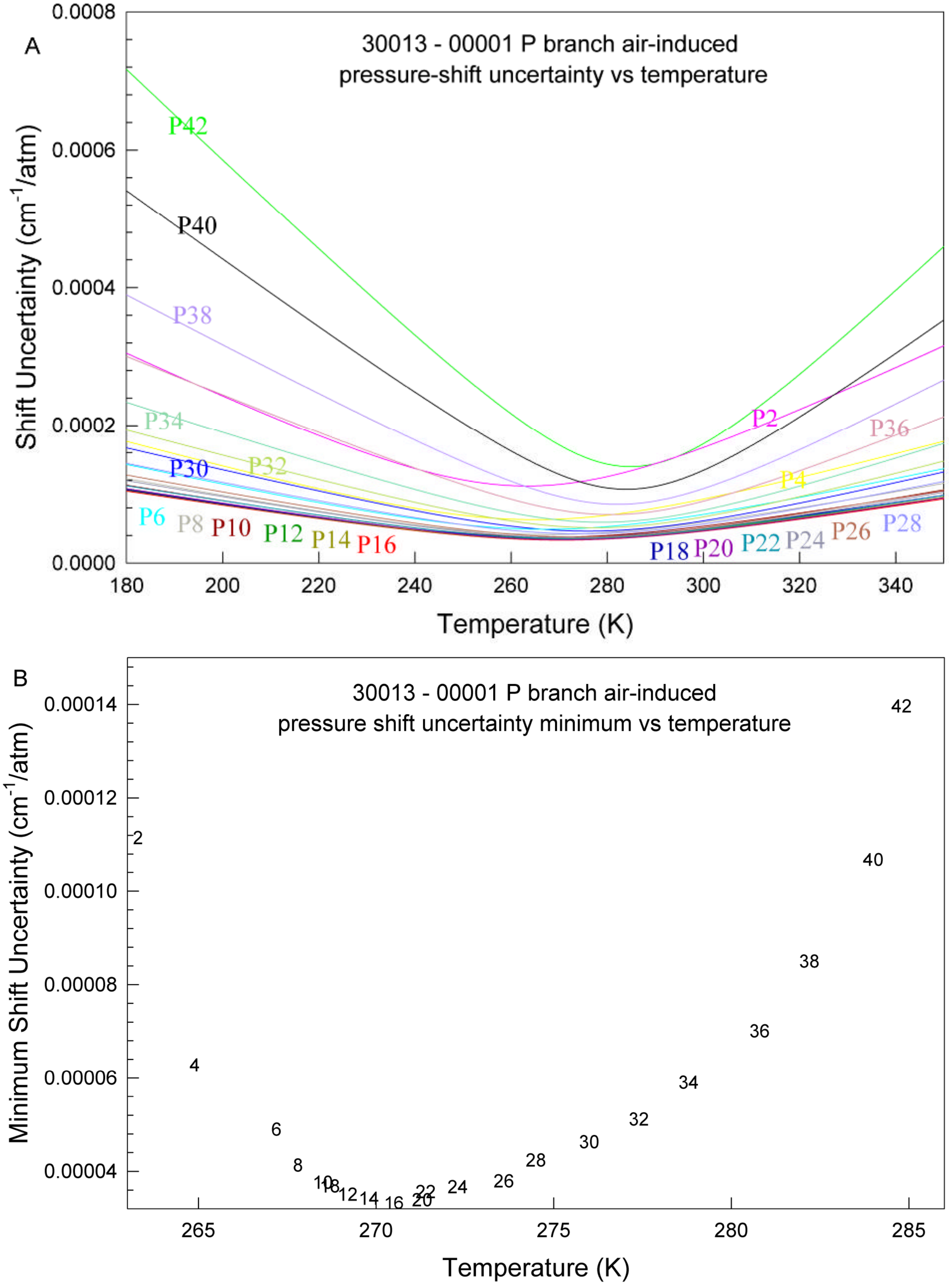
A
30013 - 00001 P branch air-induced
pressure-shift uncertainty vs temperature
Shift Uncertainty (cm^{-1}/atm)
0.0008
0.0006
0.0004
0.0002
0.0000
180
200
220
240
260
280
300
320
340
Temperature (K)
P42
P40
P38
P34
P30
P32
P2
P36
P4
P6
P8
P10
P12
P14
P16
P18
P20
P22
P24
P26
P28
B
30013 - 00001 P branch air-induced
pressure shift uncertainty minimum vs temperature
Minimum Shift Uncertainty (cm^{-1}/atm)
0.00014
0.00012
0.00010
0.00008
0.00006
0.00004
265
270
275
280
285
Temperature (K)
42
2
40
38
36
4
34
32
30
6
28
8
26
24
10
18
12
14
16
22
20

Reference	Vibrational Band	Temp. Range K	Technique	# of lines	Transitions studied	Range of n	Broadener
Aushev et al. [8]	ν_3 (emission)	T > 1000	Grating	6	R76 – R86	0.47- 0.53	Self
Aushev et al. [8]	Laser	1200 – 3000	Grating	4	P20-P26	n < 0.51	Self
Brownsword et al. [9]	ν_3	160, 298	Diode laser	5	P6-P60	Averaged 0.86 (9)	N_2
Rosenmann et al . [10]	ν_3	295 – 815	Diode laser	3	R38 –R54	0.72 -0.73	N_2
Rosenmann et al. [11]	ν_3	296 – 803	Diode laser	2	R66, R68	0.66, 0.67	N_2
Margottin-Maclou et al. [12]	ν_3	198, 296	Grating	42 1	R0-R82 (smoothed)	Ave= 0.72 R68= 0.79	N_2, O_2 Self
Margottin-Maclou et al. [12]	$\nu_1 + \nu_2$	198, 296	Grating	42	R0-R82 (smoothed)	Ave= 0.72	N_2, O_2
Planet et al. [13]	ν_2	202.2 - 297.5	Diode laser	7	Q4-Q16	0.646 - 0.831	N_2
Eng and Mantz [14]	$\nu_3 - \nu_1$ $\nu_3 -2\nu_2$	297, 387	Diode laser	1 1	P20 R18	0.943,0.827	N_2
Tettemer, and Planet [15]	ν_2 $2\nu_2 -\nu_2$	200 – 325	Diode laser	9 5	R20-R50 R19-R36	0.608 - 1.296	Self, N_2
Devi et al. [16]	ν_3 $\nu_3 +\nu_2 -\nu_2$	217-299	Diode laser	8 2	R36-R66 R46, R55	0.748-0.799	N_2
Cousin et al. [17]	ν_3	218 - 343	Grating	9	R66- R82	0.8 & 0.82	N_2, O_2
Arshinov and Leshenyuk [17]	Laser	290-600	Laser	1	R14	0.54	Self
Varanasi [18] review article	mi-IR	197-620			select lines	0.48 - 1.5	Self, N_2,O_2
Valero and Suarez [19]	$2\nu_1$ $+2\nu_2+\nu_3$	197, 233, 294	FTS	22	P2-P44 R2-R40	No values tabulated	Self, N_2, Ar
Suarez, Valero [20]	$\nu_1 +4\nu_2+\nu_3$	197, 233, 294	FTS	22	P2-P54 R4-R50	No values tabulated	Self, N_2, Ar

Pure CO_2				**CO_2 in air**			
Temp (K)	Pressure (torr)	Path [a] (m)	CO_2 (VMR)	Temp (K)	Pressure (torr)	Path [a] (m)	CO_2 (VMR)
293.9	26.10[b]	24.94	1.0	258.9	370.4	40.15	0.101
294.1	11.04[b]	24.94	1.0	258.9	249.5	40.15	0.101
CO_2 in air				258.9	153.9	40.15	0.105
292.9	923.52	121.2	0.0593	258.9	77.8	40.15	0.106
293.1	250.38	121.2	0.0595				
292.8	100.86	121.2	0.0605	244.4	709.0	80.15	0.102
293.3	551.29	49.00	0.0152				
293.1	549.55	49.00	0.0499	234.4	600.2	60.15	0.102
293.2	200.25	49.00	0.0155	234.4	450.6	60.15	0.102
293.0	100.00	49.00	0.0160	234.4	299.9	60.15	0.102
293.2	50.07	49.00	0.0749	234.4	199.9	60.15	0.104
292.9	49.79	49.00	0.0160	234.4	100.3	60.15	0.104
292.6	26.05	49.00	0.0679	234.4	59.8	60.15	0.109
292.8	25.09	49.00	0.0170				
				219.0	749.0	80.15	0.102
296.0	798.0	80.15	0.102	219.0	601.0	80.15	0.102
296.0	501.0	80.15	0.102	219.0	450.5	80.15	0.102
295.2	100.5	80.15	0.104	219.0	300.5	80.15	0.102
291.0	492.0	80.15	0.102				
				215.3	601.7	40.15	0.102
273.9	601.0	80.15	0.102	215.3	498.4	40.15	0.102
273.9	401.0	80.15	0.102	215.3	301.3	40.15	0.102
258.9	652.1	40.15	0.102				
258.9	500.8	40.15	0.103				

[a] Spectra with path lengths of 24.94, 121.2 and 49 m were recorded at ~0.011 cm^{-1} resolution with the Kitt Peak FTS; the remaining spectra were recorded at NRC with a Bomem FTS at ~0.008 to 0.009 cm^{-1} resolution.

[b] Pure natural CO_2 samples (Volume Mixing Ratio = 1 with 0.9842 $^{16}O^{12}C^{16}O$)

1 atm = 101.3 kPa = 760 torr

Line	Position[a]	Intensity[b]	b_L^0(air)[c]	%unc.	n[d]	%unc.	ρ_{b-n}	δ^0(air)[c]	unc.	δ'(air)[e]	unc.	$\rho_{\delta^0\delta'}$	SD[d,f]
P54e	6175.528178	3.4509E-25	0.06314	1.29	0.750	(F)		-0.00698	(81)	0.000000	(F)		0.100
P52e	6177.856086	4.9553E-25	0.06883	0.93	0.750	(F)		-0.00378	(63)	0.000000	(F)		0.100
P50e	6180.152596	7.0003E-25	0.06837	0.76	0.760	(F)		-0.00466	(51)	0.000000	(F)		0.100
P48e	6182.417925	9.7279E-25	0.06822	0.47	0.770	(F)		-0.00555	(32)	0.000000	(F)		0.100
P46e	6184.652290	1.3296E-24	0.06745	0.36	0.770	(F)		-0.00473	(24)	0.000000	(F)		0.060
P44e	6186.855909	1.7871E-24	0.06776	0.27	0.780	(F)		-0.00645	(17)	0.000000	(F)		0.099
P42e	6189.028995	2.3616E-24	0.06786	0.25	0.770	2.96	-0.496	-0.00690	(16)	-0.000056	(7)	+0.475	0.108
P40e	6191.171758	3.0679E-24	0.06843	0.19	0.876	1.92	-0.523	-0.00611	(12)	-0.000074	(5)	+0.497	0.088
P38e	6193.284405	3.9168E-24	0.06851	0.16	0.775	1.64	-0.544	-0.00702	(10)	-0.000059	(4)	+0.518	0.093
P36e	6195.367137	4.9131E-24	0.06886	0.13	0.798	1.25	-0.565	-0.00670	(08)	-0.000080	(3)	+0.533	0.105
P34e	6197.420146	6.0531E-24	0.06934	0.12	0.709	1.16	-0.586	-0.00654	(07)	-0.000054	(2)	+0.556	0.109
P32e	6199.443622	7.3221E-24	0.06930	0.10	0.755	0.91	-0.605	-0.00696	(06)	-0.000040	(2)	+0.570	0.105
P30e	6201.437743	8.6923E-24	0.07051	0.10	0.769	0.79	-0.623	-0.00684	(06)	-0.000051	(2)	+0.585	0.106
P28e	6203.402679	1.0121E-23	0.07059	0.08	0.763	0.71	-0.635	-0.00716	(05)	-0.000051	(1)	+0.595	0.110
P26e	6205.338591	1.1552E-23	0.07075	0.08	0.718	0.70	-0.645	-0.00697	(05)	-0.000058	(1)	+0.610	0.107
P24e	6207.245631	1.2913E-23	0.07235	0.08	0.725	0.65	-0.657	-0.00666	(05)	-0.000048	(1)	+0.622	0.129
P22e	6209.123937	1.4122E-23	0.07278	0.08	0.719	0.63	-0.660	-0.00688	(05)	-0.000058	(1)	+0.625	0.130
P20e	6210.973638	1.5090E-23	0.07427	0.07	0.703	0.61	-0.664	-0.00654	(04)	-0.000060	(1)	+0.633	0.131
P18e	6212.794851	1.5728E-23	0.07559	0.08	0.714	0.60	-0.675	-0.00664	(05)	-0.000061	(1)	+0.639	0.141
P16e	6214.587680	1.5951E-23	0.07605	0.07	0.700	0.59	-0.672	-0.00663	(04)	-0.000057	(1)	+0.642	0.126
P14e	6216.352216	1.5689E-23	0.07802	0.08	0.706	0.58	-0.678	-0.00611	(04)	-0.000061	(1)	+0.649	0.147
P12e	6218.088537	1.4892E-23	0.07968	0.08	0.677	0.61	-0.681	-0.00598	(05)	-0.000070	(1)	+0.653	0.143
P10e	6219.796708	1.3540E-23	0.08162	0.07	0.713	0.59	-0.690	-0.00601	(05)	-0.000042	(1)	+0.660	0.140
P8e	6221.476778	1.1644E-23	0.08377	0.08	0.719	0.61	-0.697	-0.00538	(06)	-0.000053	(1)	+0.667	0.132
P6e	6223.128784	9.2486E-24	0.08587	0.09	0.817	0.59	-0.711	-0.00518	(07)	-0.000056	(2)	+0.673	0.131
P4e	6224.752748	6.4331E-24	0.08711	0.11	0.687	0.86	-0.723	-0.00414	(09)	-0.000073	(2)	+0.692	0.124
P2e	6226.348677	3.3064E-24	0.09061	0.19	0.699	1.35	-0.744	-0.00479	(16)	-0.000058	(3)	+0.707	0.117
R0e	6228.689986	1.6745E-24	0.09472	0.34	0.693	2.44	-0.757	-0.00299	(31)	-0.000086	(6)	+0.717	0.091
R2e	6230.215765	4.9779E-24	0.08965	0.13	0.723	0.95	-0.736	-0.00409	(11)	-0.000062	(2)	+0.699	0.125
R4e	6231.713419	8.0947E-24	0.08493	0.09	0.701	0.73	-0.719	-0.00414	(07)	-0.000057	(2)	+0.687	0.114
R6e	6233.182890	1.0893E-23	0.08373	0.08	0.688	0.65	-0.705	-0.00437	(06)	-0.000054	(1)	+0.676	0.139
R8e	6234.624105	1.3264E-23	0.08196	0.07	0.681	0.62	-0.696	-0.00430	(05)	-0.000055	(1)	+0.668	0.137
R10e	6236.036977	1.5126E-23	0.07977	0.08	0.706	0.58	-0.690	-0.00461	(05)	-0.000050	(1)	+0.660	0.134
R12e	6237.421403	1.6431E-23	0.07824	0.06	0.715	0.56	-0.685	-0.00470	(04)	-0.000063	(1)	+0.654	0.132
R14e	6238.777268	1.7170E-23	0.07642	0.07	0.699	0.57	-0.681	-0.00502	(04)	-0.000061	(1)	+0.651	0.135
R16e	6240.104444	1.7362E-23	0.07500	0.07	0.673	0.59	-0.678	-0.00515	(04)	-0.000072	(1)	+0.649	0.127
R18e	6241.402787	1.7057E-23	0.07371	0.07	0.676	0.61	-0.676	-0.00547	(04)	-0.000071	(1)	+0.646	0.120
R20e	6242.672143	1.6326E-23	0.07293	0.07	0.686	0.61	-0.675	-0.00585	(04)	-0.000064	(1)	+0.643	0.114
R22e	6243.912344	1.5256E-23	0.07203	0.07	0.700	0.62	-0.674	-0.00605	(04)	-0.000057	(1)	+0.639	0.126
R24e	6245.123209	1.3939E-23	0.07076	0.07	0.710	0.63	-0.671	-0.00588	(04)	-0.000061	(1)	+0.633	0.108
R26e	6246.304549	1.2467E-23	0.07023	0.09	0.750	0.63	-0.668	-0.00604	(05)	-0.000057	(1)	+0.624	0.104
R28e	6247.456161	1.0925E-23	0.06930	0.09	0.697	0.73	-0.660	-0.00586	(05)	-0.000076	(1)	+0.618	0.092
R30e	6248.577833	9.3880E-24	0.06988	0.09	0.835	0.68	-0.650	-0.00620	(05)	-0.000065	(2)	+0.598	0.097
R32e	6249.669344	7.9145E-24	0.06915	0.10	0.812	0.79	-0.637	-0.00632	(06)	-0.000054	(2)	+0.586	0.086
R34e	6250.730463	6.5495E-24	0.06846	0.12	0.831	0.90	-0.619	-0.00713	(07)	-0.000038	(2)	+0.569	0.071
R36e	6251.760953	5.3223E-24	0.06857	0.13	0.754	1.21	-0.599	-0.00712	(08)	-0.000030	(3)	+0.557	0.096
R38e	6252.760567	4.2488E-24	0.06734	0.15	0.742	1.54	-0.577	-0.00611	(09)	-0.000072	(3)	+0.540	0.074
R40e	6253.729054	3.3328E-24	0.06802	0.18	0.826	1.79	-0.554	-0.00714	(11)	-0.000074	(4)	+0.519	0.076
R42e	6254.666157	2.5696E-24	0.06668	0.22	0.711	2.77	-0.532	-0.00665	(14)	-0.000064	(6)	+0.508	0.082
R44e	6255.571615	1.9476E-24	0.06671	0.24	0.770	(F)		-0.00694	(16)	0.000000	(F)		0.096
R46e	6256.445161	1.4515E-24	0.06672	0.31	0.770	(F)		-0.00892	(21)	0.000000	(F)		0.104
R48e	6257.286530	1.0639E-24	0.06801	0.43	0.760	(F)		-0.00652	(29)	0.000000	(F)		0.100
R50e	6258.095453	7.6701E-25	0.06568	0.59	0.760	(F)		-0.00240	(38)	0.000000	(F)		0.100
R52e	6258.871660	5.4396E-25	0.06727	0.83	0.750	(F)		-0.01216	(55)	0.000000	(F)		0.100

---

[a] Zero pressure line positions in cm^{-1}, calculated with rovibrational constants from in Ref.[21].

[b] Line intensities are in $cm/molecule^{-1}$ at 296 K for a natural CO_2 sample ($^{16}O^{12}C^{16}O$ fraction of 0.9842). These are calculated using the vibrational band intensity and Herman-Wallis factors [21].

[c] Measured air-broadened Lorentz half width and pressure-shift coefficients are in $cm^{-1}atm^{-1}$ at 296 K.

[d] Temperature dependence exponents of air-width coefficients as well as speed dependence (SD)parameters are unitless.

[e] the temperature dependent coefficients of air-shift coefficients are in $cm^{-1}atm^{-1}K^{-1}$.
[f] SD parameters are the same as in Ref. [21] and were fixed in the least-squares solution.

Line	Position[a]	Intensity[b]	b_L^0(air)[c]	%unc.	n[d]	%unc.	ρ_{b-n}	δ^0(air)[c]	unc.	δ'(air)[e]	unc.	$\rho_{\delta^0\delta'}$	SD[d,f]
P54	6295.319760	2.9053E-25	0.06720	1.88	0.750	(F)		-0.00370	(124)	0.000000	(F)		0.100
P52	6297.618696	4.2334E-25	0.07147	1.30	0.750	(F)		-0.00503	(92)	0.000000	(F)		0.100
P50	6299.893138	6.0610E-25	0.06776	0.90	0.760	(F)		-0.00632	(60)	0.000000	(F)		0.100
P48	6302.142651	8.5345E-25	0.06907	0.64	0.770	(F)		-0.00830	(44)	0.000000	(F)		0.100
P46	6304.366818	1.1813E-24	0.06812	0.47	0.770	(F)		-0.00667	(31)	0.000000	(F)		0.100
P44	6306.565245	1.6071E-24	0.06675	0.40	0.725	5.49	-0.504	-0.00731	(26)	-0.000020	(12)	+0.488	0.100
P42	6308.737559	2.1484E-24	0.06822	0.31	0.821	3.45	-0.524	-0.00610	(20)	-0.000047	(9)	+0.498	0.100
P40	6310.883404	2.8218E-24	0.06860	0.25	0.884	2.34	-0.546	-0.00669	(16)	-0.000050	(6)	+0.511	0.100
P38	6313.002446	3.6404E-24	0.06846	0.20	0.804	1.93	-0.571	-0.00716	(13)	-0.000070	(5)	+0.533	0.097
P36	6315.094369	4.6118E-24	0.06899	0.16	0.813	1.49	-0.593	-0.00640	(11)	-0.000077	(4)	+0.551	0.095
P34	6317.158873	5.7353E-24	0.06895	0.15	0.755	1.30	-0.615	-0.00633	(9)	-0.000077	(3)	+0.572	0.102
P32	6319.195679	6.9991E-24	0.06936	0.13	0.719	1.14	-0.634	-0.00684	(8)	-0.000059	(2)	+0.592	0.114
P30	6321.204523	8.3778E-24	0.07008	0.11	0.743	0.96	-0.650	-0.00716	(7)	-0.000057	(2)	+0.606	0.094
P28	6323.185158	9.8306E-24	0.07076	0.10	0.770	0.82	-0.662	-0.00684	(6)	-0.000065	(2)	+0.617	0.108
P26	6325.137354	1.1301E-23	0.07123	0.10	0.786	0.73	-0.671	-0.00705	(6)	-0.000062	(2)	+0.627	0.112
P24	6327.060897	1.2717E-23	0.07174	0.10	0.722	0.75	-0.676	-0.00711	(5)	-0.000049	(1)	+0.640	0.109
P22	6328.955587	1.3993E-23	0.07263	0.08	0.733	0.70	-0.681	-0.00669	(5)	-0.000057	(1)	+0.646	0.122
P20	6330.821242	1.5035E-23	0.07413	0.08	0.725	0.68	-0.684	-0.00625	(5)	-0.000069	(1)	+0.652	0.124
P18	6332.657693	1.5750E-23	0.07513	0.08	0.741	0.65	-0.688	-0.00633	(5)	-0.000066	(1)	+0.657	0.127
P16	6334.464787	1.6045E-23	0.07638	0.08	0.711	0.68	-0.693	-0.00661	(5)	-0.000057	(1)	+0.664	0.144
P14	6336.242384	1.5843E-23	0.07796	0.09	0.704	0.67	-0.696	-0.00588	(5)	-0.000071	(1)	+0.669	0.144
P12	6337.990359	1.5091E-23	0.07990	0.09	0.687	0.68	-0.701	-0.00592	(5)	-0.000070	(1)	+0.675	0.143
P10	6339.708601	1.3760E-23	0.08158	0.09	0.698	0.69	-0.709	-0.00609	(6)	-0.000050	(1)	+0.683	0.132
P8	6341.397014	1.1861E-23	0.08368	0.10	0.705	0.71	-0.721	-0.00542	(7)	-0.000058	(2)	+0.693	0.139
P6	6343.055514	9.4379E-24	0.08608	0.10	0.782	0.72	-0.738	-0.00437	(8)	-0.000072	(2)	+0.701	0.127
P4	6344.684032	6.5732E-24	0.08702	0.14	0.709	0.94	-0.751	-0.00526	(10)	-0.000069	(2)	+0.719	0.115
P2	6346.282512	3.3809E-24	0.09036	0.22	0.673	1.59	-0.770	-0.00481	(19)	-0.000071	(4)	+0.736	0.129
R0	6348.623821	1.7134E-24	0.09575	0.41	0.646	3.00	-0.782	-0.00437	(38)	-0.000072	(8)	+0.748	0.097
R2	6350.147049	5.0877E-24	0.08942	0.16	0.725	1.09	-0.762	-0.00318	(13)	-0.000068	(3)	+0.727	0.122
R4	6351.640149	8.2642E-24	0.08597	0.12	0.701	0.83	-0.745	-0.00461	(9)	-0.000055	(2)	+0.715	0.122
R6	6353.103126	1.1103E-23	0.08387	0.10	0.670	0.76	-0.730	-0.00473	(7)	-0.000055	(2)	+0.705	0.128
R8	6354.535998	1.3490E-23	0.08202	0.09	0.701	0.68	-0.720	-0.00455	(6)	-0.000051	(1)	+0.693	0.131
R10	6355.938798	1.5342E-23	0.07993	0.09	0.696	0.66	-0.713	-0.00459	(6)	-0.000057	(1)	+0.686	0.136
R12	6357.311570	1.6613E-23	0.07781	0.08	0.695	0.66	-0.707	-0.00430	(5)	-0.000070	(1)	+0.680	0.132
R14	6358.654375	1.7295E-23	0.07653	0.08	0.680	0.67	-0.704	-0.00492	(5)	-0.000063	(1)	+0.678	0.134
R16	6359.967286	1.7414E-23	0.07485	0.08	0.672	0.68	-0.701	-0.00498	(5)	-0.000083	(1)	+0.676	0.117
R18	6361.250392	1.7026E-23	0.07355	0.08	0.653	0.72	-0.699	-0.00560	(5)	-0.000068	(1)	+0.674	0.124
R20	6362.503794	1.6211E-23	0.07282	0.08	0.693	0.69	-0.700	-0.00645	(5)	-0.000065	(1)	+0.670	0.116
R22	6363.727610	1.5060E-23	0.07191	0.08	0.705	0.71	-0.701	-0.00611	(5)	-0.000061	(1)	+0.668	0.123
R24	6364.921972	1.3673E-22	0.07131	0.10	0.712	0.73	-0.699	-0.00592	(5)	-0.000062	(1)	+0.663	0.111
R26	6366.087028	1.2146E-23	0.07001	0.10	0.703	0.78	-0.696	-0.00636	(6)	-0.000052	(1)	+0.657	0.111
R28	6367.222941	1.0566E-23	0.07073	0.10	0.790	0.76	-0.692	-0.00574	(6)	-0.000086	(1)	+0.645	0.112
R30	6368.329890	9.0073E-24	0.07042	0.11	0.808	0.82	-0.681	-0.00660	(7)	-0.000063	(1)	+0.630	0.101
R32	6369.408071	7.5300E-24	0.06945	0.13	0.834	0.90	-0.667	-0.00668	(7)	-0.000052	(2)	+0.614	0.099
R34	6370.457696	6.1759E-24	0.06889	0.15	0.819	1.09	-0.650	-0.00713	(9)	-0.000027	(3)	+0.600	0.092
R36	6371.478994	4.9716E-24	0.06850	0.16	0.659	1.68	-0.634	-0.00715	(10)	-0.000035	(3)	+0.596	0.121*
R38	6372.472213	3.9295E-24	0.06798	0.19	0.733	1.88	-0.610	-0.00646	(12)	-0.000080	(4)	+0.571	0.088
R40	6373.437618	3.0503E-24	0.06898	0.23	0.821	2.21	-0.583	-0.00721	(15)	-0.000051	(5)	+0.545	0.112*
R42	6374.375493	2.3261E-24	0.06736	0.30	0.771	3.17	-0.560	-0.00612	(19)	-0.000031	(7)	+0.529	0.100
R44	6375.286142	1.7430E-24	0.06843	0.38	0.782	4.40	-0.538	-0.00667	(25)	-0.000085	(10)	+0.513	0.100
R46	6376.169887	1.2835E-24	0.06692	0.43	0.770	(F)		-0.00669	(29)	0.000000	(F)		0.100
R48	6377.027072	9.2908E-25	0.06826	0.59	0.760	(F)		-0.00608	(40)	0.000000	(F)		0.100
R50	6377.858062	6.6115E-25	0.06733	0.83	0.760	(F)		-0.00062	(55)	0.000000	(F)		0.100

---

[a] Zero pressure line positions in cm^{-1} are calculated using the rovibrational constants reported in Ref. [22]. They are listed for convenience to the reader.

[b] Line intensities in cm/molecule^{-1} at 296 K for a natural CO_2 sample ($^{16}O^{12}C^{16}O$ fraction of 0.9842) are calculated using the vibrational band intensity and Herman-Wallis factors in Ref. [22].

[c] Measured air-broadened Lorentz width and pressure-shift coefficients are in cm^{-1}atm^{-1} at 296 K.

[d] Temperature dependence exponents of air-broadened half width coefficients as well as speed dependence (SD) parameters are unitless.

[e] the temperature dependent coefficients of air-shift coefficients are in $cm^{-1}atm^{-1}K^{-1}$.

[f] SD parameters are the same as in Ref. [22] and were fixed in the present least-squares solution.

* retained in the fit.

System	**γ_{min}(cm^{-1}atm^{-1})**	**γ_{max}(cm^{-1}atm^{-1})**	**n_{min}**	**n_{max}**
CO_2-N_2	0.0496	0.0965	0.398	0.771
CO_2-O_2	0.0362	0.0728	0.185	0.787
CO_2-air	0. 0468	0.0915	0.364	0.769
CO_2-CO_2	0.0493	0.1239	0.488	0.748

Line	Width	% rms	n	% rms	shift(unc)	δ'	% error
P(54)	0.0652	3.1			-5.34(74)		
P(52)	0.0702	1.9			-4.40(56)		
P(50)	0.0681	-0.4			-5.49(39)		
P(48)	0.0686	0.6			-6.93(27)		
P(46)	0.0678	0.5			-5.70(20)		
P(44)	0.0673	-0.8			-6.88(16)		
P(42)	0.0680	0.3	0.796	3.2	-6.50(13)	-5.13	-9.1
P(40)	0.0685	0.1	0.880	0.5	-6.40(10)	-6.20	-19.2
P(38)	0.0685	0.0	0.790	1.8	-7.09(08)	-6.39	8.2
P(36)	0.0689	0.1	0.806	0.9	-6.55(07)	-7.89	-1.9
P(34)	0.0691	-0.3	0.732	3.2	-6.44(06)	-6.53	17.5
P(32)	0.0693	0.0	0.737	-2.4	-6.90(04)	-4.99	19.0
P(30)	0.0703	-0.3	0.756	-1.7	-7.00(04)	-5.36	5.6
P(28)	0.0707	0.1	0.766	0.5	-7.00(04)	-5.79	11.9
P(26)	0.0710	0.3	0.752	4.5	-7.01(03)	-6.00	3.4
P(24)	0.0720	-0.4	0.723	-0.2	-6.89(04)	-4.85	1.2
P(22)	0.0727	-0.1	0.726	0.9	-6.78(03)	-5.75	-0.9
P(20)	0.0742	-0.1	0.714	1.5	-6.40(03)	-6.42	6.8
P(18)	0.0754	-0.3	0.727	1.8	-6.48(04)	-6.36	4.4
P(16)	0.0762	0.2	0.706	0.8	-6.62(03)	-5.68	0.3
P(14)	0.0780	0.0	0.705	-0.1	-5.99(03)	-6.58	7.9
P(12)	0.0798	0.1	0.682	0.8	-5.95(04)	-6.94	0.4
P(10)	0.0816	0.0	0.706	-1	-6.05(04)	-4.63	8.6
P(8)	0.0837	-0.1	0.712	-1	-5.40(04)	-5.59	4.4
P(6)	0.0860	0.1	0.800	-2.2	-4.78(05)	-6.38	12.6
P(4)	0.0871	-0.1	0.698	1.6	-4.70(07)	-7.09	-3.2
P(2)	0.0905	-0.1	0.686	-1.9	-4.80(12)	-6.47	10.1
R(0)	0.0952	0.5	0.669	-3.6	-3.68(24)	-7.87	-8.8
R(2)	0.0895	-0.1	0.724	0.1	-3.63(09)	-6.50	4.9
R(4)	0.0855	0.6	0.701	0	-4.38(06)	-5.61	-1.3
R(6)	0.0838	0.1	0.679	-1.3	-4.55(05)	-5.46	0.4
R(8)	0.0820	0.0	0.692	1.4	-4.43(04)	-5.32	-3.8
R(10)	0.0799	0.1	0.701	-0.7	-4.60(04)	-5.33	6.7
R(12)	0.0780	-0.3	0.705	-1.4	-4.50(03)	-6.64	5.8
R(14)	0.0765	0.1	0.690	-1.4	-4.97(03)	-6.24	1.5
R(16)	0.0749	-0.1	0.672	-0.1	-5.06(03)	-7.74	7.3
R(18)	0.0736	-0.1	0.665	-1.8	-5.53(03)	-6.97	-2.1
R(20)	0.0729	-0.1	0.689	0.5	-6.15(03)	-6.46	0.9
R(22)	0.0720	-0.1	0.702	0.4	-6.08(03)	-5.90	3.0
R(24)	0.0710	0.4	0.711	0.2	-5.90(03)	-6.12	1.0
R(26)	0.0701	-0.2	0.726	-3.2	-6.20(04)	-5.46	-4.1
R(28)	0.0700	1.0	0.743	6.3	-5.80(04)	-8.08	6.5

R(30)	0.0702	0.4	0.822	-1.6	-6.40(04)	-6.41	-1.2
R(32)	0.0693	0.2	0.823	1.3	-6.50(05)	-5.28	-2.0
R(34)	0.0687	0.3	0.825	-0.7	-7.13(05)	-3.21	-17
R(36)	0.0685	-0.1	0.707	-6.7	-7.14(06)	-3.23	8.7
R(38)	0.0677	0.5	0.738	-0.6	-6.28(08)	-7.62	5.7
R(40)	0.0685	0.7	0.823	-0.4	-7.18(10)	-6.25	-19
R(42)	0.0670	0.5	0.741	4.1	-6.38(11)	-4.77	-36.1
R(44)	0.0676	1.3			-6.81(15)		
R(46)	0.0668	0.2			-7.80(18)		
R(48)	0.0681	0.2			-6.30(25)		

Width coefficients (HWHM) are in units of $cm^{-1}atm^{-1}$ at 296 K. The temperature dependence coefficients of widths (n) are unitless. The pressure shift coefficients are in 10^{-3} $cm^{-1}atm^{-1}$ at 296 K. The temperature dependents of shift coefficients (δ') are in units of 10^{-5} $cm^{-1}atm^{-1}K^{-1}$.